Published in final edited form as:
Nat Immunol. 2021 November 01; 22(11): 1403–1415. doi:10.1038/s41590-021-01047-4.

Tumor-induced reshuffling of lipid composition on the ER membrane sustains macrophage survival and pro-tumorigenic activity

Giusy Di Conza[1,2], **Chin-Hsien Tsai**[1,2], **Hector Gallart-Ayala**[3], **Yi-Ru Yu**[1,2], **Fabien Franco**[1,2], **Lea Zaffalon**[4], **Xin Xie**[5], **Xiaoyun Li**[1,2], **Zhengtao Xiao**[6], **Lydia N. Raines**[7], **Maryline Falquet**[1], **Antoine Jalil**[8], **Jason W. Locasale**[6], **Piergiorgio Percipalle**[5,9], **David Masson**[8], **Stanley Ching-Cheng Huang**[7,10], **Fabio Martinon**[4], **Julijana Ivanisevic**[3], **Ping-Chih Ho**[1,2]

[1]Department of Oncology, University of Lausanne, Epalinges, Switzerland

[2]Ludwig Institute for Cancer Research, University of Lausanne, Epalinges, Switzerland

[3]Metabolomics Platform, Faculty of Biology and Medicine, University of Lausanne, Switzerland

[4]Department of Biochemistry, University of Lausanne, Epalinges, Switzerland

[5]Program in Biology, Division of Science and Mathematics, New York University, Abu Dhabi, United Arab Emirates

[6]Department of Pharmacology and Cancer Biology, Duke University School of Medicine, Durham, USA

[7]Department of Pathology, Case Western Reserve University School of Medicine, Cleveland, USA

[8]Lipids Nutrition Cancer – LNC, INSERM- Université de Bourgogne

[9]Department of Molecular Bioscience, Wenner-Gren Institute, Stockholm University, Sweden

[10]Case Comprehensive Cancer Center, Case Western Reserve University School of Medicine, Cleveland, USA

Abstract

Correspondence to: Ping-Chih Ho.

Correspondence: Ping-Chih Ho, Department of Fundamental Oncology, University of Lausanne, Chemin des Boveresses 155, 1066 Epalinges, Switzerland, Phone: 41-0-21-692-5947, Fax: 41-0-21-314-7477, ping-chih.ho@unil.ch.

Author Contributions

G.D.C. and P.-C.H. designed the research. G.D.C, Y.-R.Y. and C.-H.T. performed *in vivo* experiment. G.D.C., Y.-R.Y., and X.L. performed *in vitro* experiments. H.G.A. and J.I. performed lipidomic experiment and analysis. F.F. performed electron microscopy analyses. L.Z., M.F. and L.N.R. performed western blot. X.X. and P.P. performed computational analysis of RNA-sequencing. A.J. and D.M. provided donor mice and bone marrow for bone-marrow transplantation experiment. Z.X. and J.L. performed computational analysis of single cell RNA-sequencing of human and murine tumor cohorts. S.C-C.H. and F.M. provided feedback and advise. G.D.C. and P.-C.H. wrote the manuscript.

Competing Interests Statement

P.-C.H. is scientific advisory for Elixiron Immunotherapeutics, Acepodia and Novartis. P.-C.H. also receive research supports from Roche and Elixiron. J.W.L. is a paid advisor to Restoration Foodworks. The remaining authors declare no competing interests.

Reporting Summary. Detailed information on experimental design is available in the Life Sciences Reporting Summary linked to this article.

Europe PMC Funders Author Manuscripts

Tumor-associated macrophages (TAMs) display pro-tumorigenic phenotypes for supporting tumor progression in response to microenvironmental cues imposed by tumor and stromal cells. However, the underlying mechanisms by which tumor cells instruct TAM behavior remain elusive. Here we uncover that tumor cell-derived glucosylceramide stimulated unconventional endoplasmic reticulum (ER) stress responses by inducing reshuffling of lipid composition and saturation on the ER membrane in macrophages, which induced IRE1-mediated spliced XBP1 production and STAT3 activation. The cooperation of spliced XBP1 and STAT3 reinforced the pro-tumorigenic phenotype and expression of immunosuppressive genes. Ablation of XBP-1 expression with genetic manipulation or ameliorating ER stress responses by facilitating LPCAT3-mediated incorporation of unsaturated lipids to the phosphatidylcholine hampered pro-tumorigenic phenotype and survival in TAMs. Together, our findings reveal the unexpected roles of tumor cell-produced lipids that simultaneously orchestrate macrophage polarization and survival in tumors via induction of ER stress responses and therapeutic targets for sustaining host anti-tumor immunity.

Introduction

In the tumor microenvironment (TME), tumor-associated macrophages (TAMs) represent one of the most abundant immune cells and are characterized by heterogenous and plastic features, giving rise to populations spanning from anti-tumorigenic towards pro-tumorigenic TAMs[1]. Anti-tumorigenic TAMs are antigen-presenting cells expressing high levels of major histocompatibility complex II (MHCII) and capable of killing tumor cells with phagocytotic activity. In addition, anti-tumorigenic TAMs can act as immuno-stimulatory cells to secrete pro-inflammatory cytokines for sustaining adaptive immunity[2]. In contrast, pro-tumorigenic TAMs are pro-angiogenic and immunosuppressive cells characterized by low expression of MHCII but produce high levels of programmed death-ligand 1 (PD-L1) and anti-inflammatory cytokines[3, 4]. Microenvironmental factors imposed by the TME, including origins of tumors, metabolic contexts, and cytokine milieus, have been suspected to tailor pro-tumorigenic features and mitigate the anti-tumorigenic ones[5], making macrophage plasticity an attractive target for therapeutic interventions. In support of this, targeting essential pro-tumorigenic genes with macrophage-specific genetic ablations have been reported to result in tremendous impacts on tumor progression and metastasis[6, 7, 8]. Tumor cells have been suggested to utilize their oncogenic and metabolic pathways for creating microenvironmental cues that orchestrate differentiation and formation of immunosuppressive and pro-tumorigenic immune cells[9, 10, 11]. Emerging evidence suggests that deregulated lipid metabolism not only enhances metastatic and invasive behavior of cancer cells[12, 13], but also contributes to the generation of a lipid-enriched TME that hampers host anti-tumor immunity and sustain survival of suppressive cells[14, 15, 16]. However, whether lipid production in tumor cells can polarize pro-tumorigenic TAMs remain largely elusive.

The ER stress response is an evolutionarily conserved mechanism to ensure survival or perish in response to stress-induced ER dysfunctions, including accumulation of misfolded proteins, impaired calcium homeostasis, and altered lipid metabolism[17]. These ER dysfunctions are sensed by three different proteins, activating transcription factor 6

(ATF6), protein kinase R-like endoplasmic reticulum kinase (PERK) and Inositol-requiring enzyme 1 (IRE1), located within the ER membrane to launch ER stress responses. The coordination of these ER stress signaling branches re-adjusts ER homeostasis through multiple mechanisms involved in transcriptional reprogramming, translational arrest, cellular macromolecule and mRNA degradation, and misfolded protein degradation[18]. ER stress, especially IRE1-mediated production of spliced form of X-box binding protein 1 (XBP1) and C/EBP jomologous protein (CHOP), has recently emerged to be responsible of promoting T cell dysfunction[19, 20], impairment of antigen presenting capacity in dendritic cells[21], and immunosuppressive phenotypes in myeloid-derived suppressor cells (MDSC)[22]. In contrast, despite that IRE1 expression in TAMs has been shown to support suppressive features and expression of PD-L1[23], how ER stress fine-tune macrophage polarization and which microenvironmental stimuli imposed by tumors are responsible for eliciting ER stress responses remain largely unknown.

Here, we show that tumor cell-produced β-glucosylceramide drives reshuffling of lipid composition on ER membrane leading to IRE1-dependent ER stress responses. As a result of co-engagement of IRE1-XBP1 and IRE1-STAT3 signal branches, this specialized ER stress response facilitates pro-tumorigenic polarization in macrophages with a strong survival capacity within the TME. We further uncover that targeting IRE1-XBP1 and IRE1-STAT3 signal branches or preserving lipid composition of the ER membrane by genetic and pharmacological approaches effectively demolish the pro-tumorigenic TAMs and restrain tumor progression. These results highlight the unexplored mechanisms controlled by ER stress responses, which allow tumor cells to manipulate macrophage properties in tumors and suggest that targeting IRE1-mediated ER stress response and lipid reshuffling are promising strategies for reprogramming the TME.

Results

TAMs display high lipid content and ER stress responses

To gain insights into lipid metabolism in TAMs, we assessed lipid content and uptake in macrophages residing in tumors and spleen with BODIPY and Fillipin III staining and uptake of BODIPY C12, a fluorescent lipid analogue, in both the YUMM1.7 melanoma engraftment murine model and a genetically engineered murine melanoma model (referred as Braf/Pten mice). In both models TAMs increased neutral lipid (BODIPY staining) and cholesterol (Flippin III staining) content and uptake compared to splenic macrophages (Fig. 1a-b and Extended data Fig. 1a-c). Moreover, lipid droplets exclusively appeared in the cytoplasm of TAMs, but not splenic macrophages (Fig. 1c). TAMs expressing arginase 1 (ARG1), one marker enzyme rendering pro-tumorigenic features in macrophages, displayed a higher lipid content compared to ARG1^{-} TAMs (Fig. 1d and Extended data Fig. 1d), suggesting that aberrant lipid accumulation driven by the tumor microenvironment (TME) may skew pro-tumorigenic properties in TAMs. In addition to formation of lipid droplets, we found that the endoplasmic reticulum (ER) of TAMs was more extended and swollen, a morphological sign of ER stress responses[24] (Fig. 1e). In support of this, TAMs increased mRNA expression of typical ER stress-responsive genes, including *Ern1, Bip* and spliced *Xbp1* (sXBP1), in both engrafted and inducible melanoma models (Fig.

2a and Extended data Fig. 1e). Moreover, we confirmed that TAMs contained a higher percentage of population expressing sXBP1 protein compared to splenic macrophages (Fig. 2b and Extended data Fig. 1f), indicating that TAMs may engage ER stress responses. Since emerging studies suggested the crosstalk between deregulated lipid metabolism and ER stress can play a vital role on tailoring cellular behavior in metabolic tissues[17], we then examined the expression of sXBP1 with lipid contents and ARG1 in TAMs. sXBP1$^+$ TAMs had higher lipid contents (Fig. 2c and Extended data Fig. 1g) and represented the majority of pro-tumorigenic TAM subset, characterized by ARG1 expression (Fig. 2d and Extended data Fig. 1h-i). To confirm these findings in a more physiologically relevant setting, we compared the expression of sXBP1 and lipid content between TAMs and skin-resident macrophages from Braf/Pten melanoma-bearing and found that both parameters were higher in TAMs (Extended data Fig. 1j-l). By computationally weighting ER stress responses of individual TAMs from the published single cell RNA sequencing results of several human cancers, including colorectal cancer (CRC)[25], lung adenocarcinoma without chronic obstructive pulmonary disease (LUAD-No COPD) and Non-small cell lung carcinoma (NSCLC)[26, 27], and a cohort of murine sarcoma[28], we observed that pro-tumorigenic TAMs displayed higher ER stress scores compared to anti-tumorigenic TAMs (Fig. 2e). Importantly, despite TAMs expressed higher amounts of sXBP1, we only observed slightly increase of phosphorylated-PERK staining and decreased expression of ATF6 target genes, including *Herpud1* and *Derl1,* compared to splenic macrophages (Extended data Fig. 1m-n). These results indicate that TAMs preferentially engage XBP1-mediated ER stress responses. Taken together, our data highlight that ER stress and deregulated lipid metabolism may coordinate to tailor pro-tumorigenic features of TAMs.

IRE1-XBP1 reinforces macrophage pro-tumoral polarization

To investigate whether tumor cell-derived factors could stimulate increased lipid content and ER stress responses in macrophages, we treated bone marrow-derive macrophages (BMDMs) with YUMM1.7 tumor cell-derived conditioned medium (CM). Our results showed that CM promoted both lipid content and uptake (Fig. 3a and Extended data Fig. 2a), accompanying with elevated expression of pro-tumorigenic marker genes, including *Arg1* and mannose receptor C-type I (*Mrc1*), but declined expression of anti-tumorigenic marker genes (Fig. 3b and Extended data Fig. 2b-d). Moreover, CM-treated BMDMs showed increased activity on suppressing proliferation of CD8$^+$ T cells compared to naïve macrophages (Extended data Fig. 2e). Despite that interleukin-4 (IL-4)/interleukin-13 (IL-13) neutralizing antibodies treatment abrogated IL-4/IL-13 induced alternative activation in BMDMs (Extended data Fig. 2f), these neutralizing antibodies failed to prevent CM-induced expression of pro-tumorigenic marker genes (Extended data Fig. 2g) and the quantity of IL-4 and IL-13 in YUMM1.7 CM were lower than the detection limit (Extended data Fig. 2h). In addition, CM derived from non-transformed murine embryonic fibroblast (MEF) was unable to increase lipid content and expression of pro-tumorigenic marker genes in BMDMs (Extended data Fig. 2i-k). These results indicate that tumor cells could preferentially increase lipid content and pro-tumorigenic polarization in macrophages via an IL-4/IL-13-indpendent manner.

Interestingly, CM-treated BMDM showed production of sXBP1, but minimal increase of PERK activation (based on mobility shift in immunoblot) and PERK downstream target, activating transcription factor 4 (ATF4) (Fig. 3c). Moreover, CM failed to stimulate expression of ATF6 target genes, including *Herpud1* and *Derl1* (Extended data Fig. 2l), suggesting a preferential activation of the IRE1-XBP1 branch. Given that ER stress responses recently have been revealed to hamper anti-tumor immunity by modulating functionality of $CD8^+$ T cells, dendritic cells and MDSCs[19, 20, 21, 22], we speculate that CM-mediated activation of IRE1-XBP1 signaling might support acquisition of pro-tumorigenic phenotypes in macrophages. To test this postulate, we treated CM-stimulated BMDMs with STF081030, an inhibitor of the endoribonuclease activity of IRE1 that can prevent production of sXBP1 and found that STF081030 effectively suppressed expression of sXBP1 and pro-tumorigenic marker genes caused by CM (Fig. 3d). Furthermore, STF081030 treatment effectively ameliorated the suppressive ability in CM-treated BMDMs (Fig. 3e) and CM-boosted lipid accumulation was also dampened by STF081030 (Extended data Fig. 2m). To confirm the contribution of IRE1 in inducing pro-tumorigenic polarization, we transduced BMDMs generated from LysM-Cre Cas9 mice[29] with lentivirus harboring either scramble guide RNAs (gRNAs) or IRE1-targeting gRNAs to generate control BMDMs or IRE1-deficient BMDMs, respectively. IRE1 expression was lower in IRE1-deficient BMDMs compared to control BMDMs (Extended data Fig. 2n), and CM-induced pro-tumorigenic polarization was compromised in IRE1-deficient BMDMs (Fig. 3f), suggesting that induction of IRE1 activity by CM reinforces pro-tumorigenic polarization in macrophages. Conventional ER stress inducers, including tunicamycin and thapsigargin, were capable to induce ER stress response, but failed to polarize BMDMs towards a pro-tumorigenic phenotype (Fig. 3g and Extended data Fig. 2o), implying that specialized signaling cascades controlled by sXBP1 rather than conventional ER stress response are needed for reinforcing immunosuppressive activities in macrophages in response to tumor cell-derived factors.

XBP1 remodels TAM phenotype and supports tumor progression

To further elucidate the contribution of XBP1 on pro-tumorigenic polarization in macrophages, we transduced BMDMs generated from LysM-Cre Cas9 mice with lentivirus harboring either scramble gRNAs or XBP1-targeting gRNAs to generate control BMDMs or XBP1-deficient BMDMs, respectively. Both total and spliced XBP1 expression were decreased in XBP1-deficient BMDMs compared to control BMDMs (Extended data Fig. 3a). We found that CM-induced expression of pro-tumorigenic marker genes were reduced in XBP1-deficient BMDM compared to control BMDMs (Fig. 4a). To investigate whether the expression of XBP1 modulates pro-tumorigenic features in TAMs, we first generated myeloid cell-specific XBP1-deficient mice (designated as $XBP1^{cko}$) by crossing $Xbp1^{fl/fl}$ mice with LysM-Cre mice and $Xbp1^{fl/fl}$ mice were referred as wild-type (referred as $XBP1^{wt}$) mice. We further found that suppressive activity as well as lipid accumulation were reduced in XBP1-deficient BMDM compared to WT BMDMs (Fig. 4b and Extended data Fig. 3b). These data highlight a role of XBP1 in skewing macrophages towards pro-tumorigenic phenotype upon exposure to tumor-derived components. We next engrafted YUMM1.7 melanoma cells expressing ovalbumin peptide (YUMM1.7-OVA) into wild-type mice or $XBP1^{cko}$ mice and found that genetic ablation of *Xbp1* in myeloid cells suppressed

tumor growth (Fig. 4c-d) accompanied with a significant loss of macrophages within the TME (Extended data Fig 3c). We next applied anti-CSF1R antibody treatment to deplete macrophages in tumor-bearing wild-type or XBP1^{cko} mice to elucidate whether macrophages are responsible for the differential tumor growth rates in wild-type or XBP1^{cko} mice. Wild-type or XBP1^{cko} mice displayed similar tumor growth rates and tumor burdens upon treatment with anti-CSF1R antibody (Extended data Figure 3d-f), suggesting that XBP1 expression is required for promoting tumor progression by supporting accumulation and survival of TAMs. In agreement with previous reports[30, 31], in Ly6G^{-} myeloid cell populations, we observed a population of F4/80^{+} macrophages that express intermediate levels of Ly6C (refereed as immature TAMs, iTAMs) which was absent in spleen of YUMM1.7-OVA-engrafted mice (Extended data Fig. 3g) and melanoma-bearing Braf/Pten mice (Extended data Fig. 3l). iTAMs expressed much higher levels of sXBP1, PD-L1 and ARG1 but lower levels of MHCII compared to the F4/80^{+} Ly6C^{-} population (designated as mature TAMs, mTAMs) (wild-type or XBP1^{cko} mice Extended data Fig. h-p), implying that ER stress responses, particularly IRE1-XBP1 branch, are engaged in the suppressive iTAM subset. By examining TAMs in both wild-type mice and XBP1^{cko} mice, our result showed that XBP1 deficiency led to changes in the abundance of mTAMs and iTAMs and a reduced ratio of iTAMs to mTAMs (Fig. 4e), suggesting that ablation XBP1 could ameliorate pro-tumorigenic feature in TAMs. Similar to YUMM1.7-OVA melanomas, we found that genetic ablation of XBP1 in myeloid cells suppressed growth of B16 melanoma overexpressing ovalbumin (Extended data Fig. 3q-r) and led to a reduction trend in tumor growth of MC38 colon adenocarcinoma overexpressing ovalbumin (Extended data Fig. 3s-t). Collectively, these results reveal that the expression of XBP1 propels TAMs towards pro-tumorigenic activation and renders survival advantage in tumors.

STAT3 signal optimizes macrophage protumoral polarization

Next, we sought to test whether the expression of sXBP1 alone is sufficient to promote M2 phenotype. Our result showed that STF083010 treatment suppressed CM-induced expression of pro-tumorigenic marker genes in control BMDMs, but not BMDMs overexpressing sXBP1 (Fig. 5a), supporting our conclusion that IRE1-mediated production of sXBP1 is needed to reinforce pro-tumorigenic activity in macrophages stimulated with CM. However, overexpression of sXBP1 was unable to induce the expression of M2 genes in Ctrl-treated BMDM (Fig. 5a), indicating that other signaling cascades that coordinate with IRE1-XBP1 pathway might be required for skewing pro-tumorigenic polarization in macrophages. A recent study revealed that STAT3 activation promotes tumor progression by triggering cathepsin expression in TAMs[32]. Indeed, we found that phosphorylated STAT3 was strongly upregulated by CM (Fig. 5b). We speculated that STAT3 activation is also needed to reinforce pro-tumorigenic polarization in response to tumor cell CM. In support of this postulate, genetic ablation of STAT3 or treatment with STAT3 inhibitor, Stattic, hampered the expression of MRC1 gene, but not ARG1, highlighting the possibility of a partial contribution of STAT3 activation to the suppressive activity of CM-treated BMDMs (Fig. 5c and Extended data Fig 4a-c). Next, we examined whether tumor cell could activate STAT3 in BMDMs via IL-6 and IL-10 production[33]. However, IL-6 and IL-10 were undetectable in melanoma cell CM (Extended data Fig 4d). Moreover, neutralizing antibodies against IL-6 and IL-10 were unable to suppress CM-induced STAT3 phosphorylation (Fig. 5d) and

the expression of pro-tumorigenic marker genes (Fig. 5e), while the doses of neutralizing antibodies we used were able to abrogate the STAT3 phosphorylation induced by IL-6 and IL-10 (Fig. 5d). These results suggest that a tumor cell-derived factor activates STAT3 for skewing pro-tumorigenic polarization in macrophages in an IL-6/IL-10-independent manner. IRE1 has been shown to support STAT3 activation in hepatocytes by forming a protein complex with STAT3[34]. By using proximity ligation assay, we found that CM facilitated IRE1-STAT3 interaction in BMDMs (Fig. 5f). We then tested whether IRE1 is needed for STAT3 phosphorylation and found that tumor cell CM-induced STAT3 phosphorylation was dampened in IRE1-deficient BMDMs compared to control BMDMs (Fig 5g). However, pharmacological inhibition of the endoribonuclease activity of IRE1 with the STF083010 did not prevent CM-induced STAT3 phosphorylation, indicating that the effect is independent of sXBP1 production (Extended data Fig. 4e). In contrast to CM, tunicamycin was not able to induce STAT3 phosphorylation, suggesting that CM activates an unconventional and mild ER stress responses that activates STAT3 in an IRE1-dependent manner (Extended data Fig. 4f). Taken together, our results suggest that CM-triggered IRE1 signal leads to pro-tumorigenic polarization in macrophages by simultaneously stimulating STAT3 activation and production of sXBP1.

Glucosylceramide sensing by Mincle tailors macrophage activation

Since aberrant lipid metabolism has been suggested to elicit ER stress response[35, 36], we postulated that lipids generated by tumor cells may be responsible for the induction of pro-tumorigenic features in macrophages. To test this, we deprived lipids, including cholesterol and fatty acids, from YUMM1.7 melanoma cell CM with a lipid removal agent (Extended data Fig. 5a-b). We found that lipid removal abolished CM-triggered production of sXBP1, STAT3 phosphorylation, and the expression of pro-tumorigenic marker genes (Fig. 6a-c). By examining the transcriptomic changes induced by CM treatment, we found that most genes responsible for pro-tumorigenic activity in macrophages were upregulated by tumor cell CM in a lipid-dependent manner (Fig. 6d). Together, these results suggest that lipids produced by tumor cells may control the engagement of ER stress responses for polarizing pro-tumorigenic activation in macrophages. Given that cholesterol was largely deprived with the lipid removal procedure, we speculated that cholesterol produced by tumor cells is responsible for pro-tumorigenic activation in macrophages. We found that CM produced from YUMM1.7 melanoma cells expressing shRNAs against 3-hydroxy-3-methyl-glutaryl-CoA reductase (HMG-CoA reductase), which controls cholesterol synthesis, remained effective to skew pro-tumorigenic polarization in BMDMs (Extended data Fig. 5c-d). Since CD36, a lipid transporter responsible for oxidized lipoproteins and long-chain fatty acid uptake, has been discovered to promote alternative activation in macrophages and lipid accumulation in TAMs[37, 38], we then tested whether blocking CD36-mediated uptake of cholesterol and long-chain fatty acid could ameliorate pro-tumorigenic polarization in BMDMs. However, treatment with a neutralizing anti-CD36 antibody[14] failed to prevent CM-induced expression of sXBP1 and pro-tumorigenic marker genes (Extended data Fig. 5e). Altogether, these results suggest that cholesterol produced by tumor cells is not involved in tumor cell CM-mediated pro-tumorigenic activation in macrophages.

By examining transcriptomic analysis with a particular focus on genes involved in lipid recognition and binding that were significantly upregulated by tumor cell CM, we found that macrophage inducible Ca^{2+}-dependent lectin receptor (Mincle), also known as C-Type lectin domain family 4 member E (Clec4e), was significantly induced by CM. The induction of Mincle protein expression in BMDMs treated with CM was further validated by flow cytometry (Fig. 6e). In addition to acting as a pattern recognition receptor to tailor macrophage activities[39, 40], Mincle has recently been reported to induce ER stress responses and facilitate lipid accumulation by inhibiting cholesterol efflux in macrophages residing in atheromas and during kidney injuries[41, 42]. To test whether Mincle-mediated lipid recognition is responsible for CM-induced changes in macrophages, we stimulated BMDMs with YUMM1.7 CM in the absence or presence of anti-Mincle antibody, which can block lipid recognition ability of Mincle. We found that anti-Mincle antibody treatment compromised activity of CM-stimulated BMDMs on hampering $CD8^+$ T cell proliferation and lipid accumulation (Fig. 6f and Extended data Fig. 5f). In addition, the CM-induced expression of sXBP1, pro-tumorigenic marker genes and STAT3 phosphorylation were ameliorated by anti-Mincle antibody treatment (Fig. 6g-h). By exploiting genetic approach, we further confirmed that CM induced less pro-tumorigenic polarization, including declined STAT3 activation, expression of sXBP1, pro-tumorigenic genes and suppressive activity, in Mincle-deficient BMDMs (Mincle-KO) compared to wild-type BMDMs (Extended data Fig. 5g-i). Together, these results indicate that Mincle-mediated lipid recognition is responsible for CM-induced pro-tumorigenic polarization in macrophages. Since β-glucosylceramide and cholesterol sulfate are the known endogenous ligands of Mincle[43] and CM derived from HMG-CoA-deficient tumor cells remained effective on modulating macrophage phenotype (Extended data Fig. 5d), we thus sought to examine whether the production of β-glucosylceramide in YUMM1.7 cells is needed to drive CM-induced pro-tumorigenic polarization in BMDMs. We expressed short hairpin RNAs (shRNAs) targeting UDP-glucose ceramide glucosyltransferase (UGCG), the metabolic enzyme responsible for β-glucosylceramide production, which resulted in effective reduction of UGCG expression and β-glucosylceramide production in YUMM1.7 melanoma cells (Fig. 6i and Extended data Fig. 5j). We found that CM derived from UGCG-deficient YUMM1.7 cells was less efficient to boost expression of sXBP1, pro-tumorigenic marker genes and STAT3 activation in BMDMs compared to CM produced from control group (Fig. 6j-k). Moreover, anti-Mincle antibody did not further suppress expression of pro-tumorigenic genes in BMDMs stimulated with CM derived from UGCG-deficient YUMM1.7 cells (Extended data Fig. 5k), suggesting that β-glucosylceramide is the bioactive component sensed by Mincle in macrophages. We also found that tumor interstitital fluids in engrafted YUMM1.7 melanomas and inducible Braf/Pten melanomas contained more β-glucosylceramide compared to serum in tumor-bearing mice (Extended data Fig. 5l-m). Moreover, UGCG deficiency in YUMM1.7 melanoma cells led to declined tumor growth (Fig. 6l-m) accompanied with a decreased ratio of iTAMs to mTAMs (Fig. 6n). Altogether, these results imply that β-glucosylceramide produced by tumor cells triggers ER stress responses in a Mincle-dependent manner for unleashing pro-tumorigenic activities in TAMs.

Disturbed lipid composition on ER membrane activates sXBP1

Since Mincle activation has been shown to inhibit cholesterol efflux and TAMs accumulate higher levels of cholesterol, we speculated that CM may promote accumulation of intracellular cholesterol by stimulating cholesterol synthesis. In support of this, we found that CM increased intracellular cholesterol in BMDMs as measured by Fillipin III staining. However, treating statin to block cholesterol synthesis and anti-Mincle antibody effectively hampered CM-induced accumulation of cholesterol (Fig. 7a). In addition, blocking cholesterol synthesis with statin prevented CM-induced expression of sXBP1 and pro-tumorigenic marker genes in BMDMs (Fig. 7b). Anti-Mincle treatment failed to further suppress CM-induced expression of sXBP1 and pro-tumorigenic marker genes in BMDMs treated with statin. These results suggest that Mincle activation orchestrates pro-tumorigenic polarization in macrophage by enhancing cholesterol synthesis. IRE1 contains a transmembrane domain that can sense lipid disbalance and induces its dimerization and activation[44] and increased cholesterol accumulation might reshuffle lipid composition of the ER membrane towards a low phosphatidylcholine (PC) to phosphatidylethanolamine (PE) ratio (PC/PE ratio) and decreased polyunsaturated fatty acid (PUFA), which can decrease ER membrane fluidity, as a result of disturbed cholesterol-sensing mechanism[45]. Thus, we hypothesized that tumor cell CM triggers IRE1/XBP1 activation by reshuffling lipid composition on ER membrane. Lipid profiling of ER membrane showed that PC/PE ratio was significantly decreased in CM-treated BMDMs compared to control group (Fig. 7c). Furthermore, we observed decreased abundances of polyunsaturated, but elevated saturated, PC in CM-stimulated BMDMs, especially palmitoyl (16:0) and linoleoyl (18:2)-containing PC (Fig. 7d-e). We then attempted to rescue the disturbed lipid composition on ER membrane by overexpressing lysophosphatidylcholine acyltransferase 3 (LPCAT3), an enzyme responsible for synthesizing phosphatidylcholine that preferentially contain unsaturated FA as acyl chains[46] and has been shown to restrict lipid overloading induced ER stress responses in hepatocytes[36]. In support of our postulate, LPCAT3 overexpression reduced both PC/PE ratio and the abundance of unsaturated PC on ER membrane in CM-stimulated BMDMs (Fig. 7f-h). By examining ER morphology with electronic microscopy analysis, we observed that LPCAT3 overexpression reduced the extension of ER membrane in BMDMs treated with melanoma cell CM, but not regular culture media (Fig. 7i), suggesting that forcing LPCAT3 expression could ameliorate CM-induced ER stress in macrophages. Furthermore, LPCAT3 overexpression could prevent CM-induced expression of sXBP1 and pro-tumorigenic marker genes in BMDMs (Figure 7j-l). Collectively, these data uncover that tumor-induced reshuffling of lipid composition on ER membrane is critical for launching the ER stress-mediated pro-tumorigenic polarization and LPCAT3-driven lipid metabolism can be a promising strategy to tailor macrophage behavior by intervening this unique ER stress induction mechanism.

LXR agonist controls tumor burden via LPCAT3 in macrophages

Since previous studies revealed that the expression of LPCAT3 is controlled by the liver X receptor (LXR)[36, 47], we then sought to pharmacologically induce the expression of LPCAT3 with GW3965, a LXR agonist, and investigate whether this treatment can be exploited to tailor functionality of TAMs. Our result showed that treatment with GW3965 resulted in LPCAT3 induction in CM-treated BMDMs (Fig. 8a) accompanied with reduced

expression of sXBP1 and STAT3 phosphorylation (Fig. 8b-c). In addition, GW3965 restrained the expression of *Arg1* and *Mrc1* induced by YUMM1.7 CM (Fig. 8d) and partially hampered the suppressing activity of CM-treated BMDMs towards $CD8^+$ T cells (Fig. 8e), indicating that GW3965 can prevent the engagement of ER stress-mediated pro-tumorigenic polarization in response to tumor cell-derived stimulation as we observed in the BMDM overexpressing LPCAT3. In addition, GW3965 failed to ameliorate CM-induced sXBP1 expression, STAT3 activation as well as suppressive activity on controlling $CD8^+$ T cell proliferation, in LPCAT3-deficient BMDMs (Extended data Fig. 6a-c). Next, we investigated whether exploiting GW3965 treatment can hamper tumor progression. Similar to a recent report[48], we found that treating tumor-bearing mice with GW3965 effectively restricted tumor growth (Fig. 8f-g). In order to address whether the anti-tumor responses we observed was dependent on LPCAT3 expression in macrophages, we generated bone-marrow (BM) transplanted mice in which lethally irradiated C57BL/6 recipient mice were transplanted with BM from either *Lpcat3* $^{fl/fl}$ mice (designated as wild-type mice, WT) or LysM-Cre *Lpcat3* $^{fl/fl}$ mice (designated as LPCAT3-knockout mice, KO) (Extended Data Fig. 6d). In this setting we could evaluate whether LPCAT3 expression in macrophages is required for GW3965-induced anti-tumor immunity. Genetic deletion was confirmed by examining the expression of exon 3 of LPCAT3 that is flanked by LoxP sequence in WT and KO BMDMs (Extended Data Fig. 6e). GW3965 potently dampened tumor growth in WT mice but failed to elicit anti-tumor responses in KO mice, indicating that GW3965-triggered anti-tumor effects rely on LPCAT3 expression in macrophages (Fig. 8h-i). Interestingly, like XBP1-deficient mice, GW3965 treatment induced a reduction of macrophage population in tumors from WT mice, but not KO mice (Fig. 7j). We did not detect changes in abundances of macrophages and other myeloid cells in bone marrow between WT and KO mice (Extended data Fig. 6f). Moreover, we observed that GW3965 treatment led to a significant reduction of iTAM population and a mild decrease of mTAMs (Fig. 7k and Extended data Fig. 6g). In addition, GW3965 treatment mitigate sXBP1 levels in iTAMs of WT mice, but not LPCAT3-deficient chimeric mice (Fig. 8l). Collectively, in line with our previous data obtained from XBP1-deficient mice, our results suggest that ER stress responses, especially sXBP1 expression, is needed for survival and pro-tumorigenic polarization in TAMs and LXR-mediated LPCAT3 induction in macrophage can be exploited for re-awakening anti-tumor responses.

Discussion

ER stress has emerged as a critical regulatory circuit to modulate immune cells within the TME; however, the stimuli imposed by tumor cells for eliciting ER stress in macrophages and how ER stress tailor functionalities of TAMs remains elusive. Here, we uncover that tumor cells promote a Mincle-mediated ER stress response to orchestrate pro-tumorigenic polarization in TAMs. We further demonstrate that reshuffling of lipid composition on ER membrane simultaneously activates IRE1-XBP1 and IRE1-STAT3 signal branches to reinforce pro-tumorigenic properties and survival in macrophages. Moreover, promoting PC synthesis and incorporation of unsaturated fatty acids into PC on ER membrane to improve fluidity can restrain pro-tumorigenic features and survival in TAMs. Together, our findings unravel the underexplored mechanisms by which tumor cells modulate macrophage

behavior and warrant development of treatments targeting lipid metabolism in macrophages for cancer therapy.

Our results show that myeloid cell-specific XBP1-deficient mice ($XBP1^{cko}$) contain less macrophages in tumor immune infiltrates and display a differential TAM profile compared to WT mice. Since sXBP1 is known to promote PC synthesis for ameliorating amplitudes of ER stress and supporting cell survival in response to perturbations of ER homeostasis[35], it is likely that the high expression of sXBP1 in macrophages promotes their survival and PC synthesis when encountering metabolic perturbations imposed by the TME. As a trade-off of sXBP1-supported survival, the accumulation of sXBP1 can launch pro-tumorigenic polarization in macrophages. In support of this possibility, our results show that LXR agonist-induced LPCAT3 expression in macrophages results in less pro-tumorigenic polarization, but decreased survival of iTAMs (the TAM population expressing the highest level of sXBP1). Moreover, pro-tumorigenic TAMs have been speculated to engage unique metabolic programs that can sustain their metabolic needs in the TME[49]. Thus, it is also likely that the metabolic properties engaged during pro-tumorigenic polarization may coordinate with sXBP1-mediated metabolic regulations to fine-tune the amplitude of ER stress for ensuring survival of macrophages in response to metabolic insults, such as lipid overloading and glucose deprivation, in tumors. Therefore, it is of interest to examine the differences of metabolic properties between iTAMs and mTAMs and explore how these differentially engaged metabolic processes can support survival of TAMs in coordination with sXBP1-mediated regulations. The understanding of this question will be warranted for development of new interventions allowing to target pro-tumorigenic TAMs but preserve anti-tumorigenic TAMs.

Although activation of IRE1-XBP1 and IRE1-STAT3 signal branches are critical for skewing pro-tumorigenic macrophages, it remains unknown whether and how sXBP1 and STAT3 work synergistically to induce functional switch towards pro-tumorigenic phenotype. In addition to modulate transcriptional program, STAT3 has been shown to modulate metabolic reprogramming in numerous cell types via non-transcriptional events[50]. Thus, it is possible that both STAT3-mediated metabolic reprogramming and transcriptional modulations can be involved in the coordination with XBP1 on tailoring macrophage polarization. Moreover, our results show that CM promotes IRE1-STAT3 protein complex formation and genetic ablation of IRE1 abolishes CM-induced STAT3 activation. However, IL-6 has been shown to activate IRE1 via a STAT3-dependent manner that in turn promotes the secretion of cathepsin protease[32]. Thus, these findings also highlight that a positive feedback loop between IRE1 and STAT3 may exist in TAMs by integrating tumor cell-derived β-glucosylceramide and IL-6 produced by stromal and tumor cells. Thus, identifying the molecular mechanisms controlled by the synergistic actions between XBP1 and STAT3 would provide critical information for targeting and, even reprogramming, pro-tumorigenic TAMs. IRE1 has been shown recently to support suppressive activity of polymorphonuclear MDSCs in tumors[51], which further warrants the therapeutic potential on harnessing IRE1targeting strategy for cancer treatment.

Our results reveal that TAMs preferentially engage the production of sXBP1 and display less activation of PERK and ATF6 signal branches. Moreover, despite that conventional ER

stress inducers, including tunicamycin and thapsigargin, stimulate all three signal branches of ER stress, tunicamycin and thapsigargin fail to promote pro-tumorigenic polarization in macrophages. In fact, it has been suspected that ER stress induced by disturbed lipid homeostasis on ER membrane is different from ER stress induced by conventional ER stress inducers, such as tunicamycin and thapsgargin, on modulating cellular behavior[52]. In contrast to conventional ER stress inducer tunicamycin which activates all three ER stress signal pathways (IRE1, ATF6 and PERK), we find that CM stimulation has no impact on the expression of ATF6 target genes. Moreover, CM treatment, but not tunicamycin stimulation, induces STAT3 phosphorylation. These results suggest that CM may induce low grade ER stress which can preferentially engage IRE1-XBP1 axis and less impact on PERK and ATF6. As a result of this specialized engagement of signaling axis, it is likely that CM may orchestrate pro-tumorigenic polarization in BMDMs. In contrast, conventional ER stress inducers simultaneously activate all three signaling arms, in which the integration of three signal axes may avoid pro-tumorigenic polarization but trigger survival and translational arrest in BMDMs by inducing a different array of downstream events. Together, these findings imply that specialized ER stress-sensing mechanism that can differentiate amplitude and stress initiation events may participate to tailor the differentiation and survival in macrophages. Therefore, elucidating how ER stress responses are engaged for dictating cellular programs in macrophages as well as other immune cells represents an important avenue for tailoring ER stress responses in cancer treatments.

Methods

Mice

C57BL/6/J and LysM-Cre (B6.129p2-*Lyz2*tm1(cre)lfo/J) mice were purchased from Jackson Laboratory and housed in the animal facility of University of Lausanne. Macrophage-specific Cas9 knock-in were generated as previously described[29]. Macrophage-specific XBP1 Knockout mice were generated by crossing LysM-Cre mice (myeloid-specific overexpression of Cre recombinase) with XBP1$^{fl/fl}$ mice. Macrophages-specific Lpcat3 knockout mice were generated by crossing LysM-Cre mice with Lpcat3$^{fl/fl}$ mice[53]. BRafCA; Tyr::CreER; Ptenlox4-5 (Braf/PTEN) was obtained from M. Bonsenburg at Yale University. Bone marrow of Mincle-knockout mice was provided by David Sancho[54]. All experiments were performed in accordance with Swiss federal regulations and procedures ethically approved by veterinary authority of Canton Vaud.

Cell lines and in vitro culture

The YUMM1.7 melanoma cell line was provided by M. Bosenberg as described previously[55]. The MEF (murine embryonic fibroblasts) were provided by F. Martinon. The YUMM1.7-OVA and B16-OVA cell line was established as described before[56] and were maintained in high-glucose DMEM (Life Technologies) with 10% fetal bovine serum (FBS, Gibco), 100 U ml–1 penicillin–streptomycin (ThermoFisher Scientific) and puromycin (InvivoGen). The YUMM1.7 shCTRL and shUGCG were established by stable transduction of parental cell line with lentivirus PLKO.1 (Addgene) carrying the short hairpins targeting scramble or UGCG sequence and were maintained in high-glucose DMEM with 10% FBS, 100 U ml–1 penicillin–streptomycin and puromycin. The MC38-OVA were provided

by P. Romero. Bone marrow cells were collected and cultured in high-glucose DMEM supplemented with 10% FBS and 20% L929 cell culture supernatant for macrophage differentiation for 6 days. On day 6, differentiated BMDMs were seeded with DMEM (without L929 cell culture supernatant) for 4h. Then, cells were stimulated as described in figure legends. For the experiments with BMDMs generated from Mincle-knockout and LPCAT3-knockout mice, bone marrow was isolated and frozen. Then, bone marrow cells were thawed and cultured in presence of DMEM supplemented with 20% FBS and 20% L929 medium for 7 days. At day 7, BMDMs were seeded and treated as described in figure legends. YUMM1.7 cancer cell-conditioned medium was collected by incubating YUMM1.7 cells (70% density) with the DMEM 10%FBS for 24h. Then, culture medium was collected and filtered through 0.22μM filters to remove cell debris and used as CM (conditioned medium). In order to generate CM without lipids, CM collected as described above was treated with Cleanascite reagent (Biotech Support Group) according to the manufacturer's instructions.

Plasmids and reagents

The retroviral vector MSCV-sXBP1-Thy1.1 and MSCV-LPCAT3-Thy1.1 was constructed by PCR cloning. The sXBP1 cDNA was amplified by PCR from the vector pFLAG.XBP1pCMV2 (Addgene), and LPCAT3 cDNA was amplified from the vector LPCAT3-pCXN2[57] (kindly provided by Dr. J. Miyazaki). Both cDNAs were insert into the MSCV-Thy1.1 between BlgII and SalI restriction sites. The MSCV-Thy1.1 is a gift from S. Kaech (Salk Institute for Biological Studies). For CRISPR–Cas9-mediated depletion, guide RNAs were cloned into pSUPER-pU6-Thy1.1 plasmid by Bbs1. The retroviral pSUPERpU6-Thy1.1 backbone vector was kindly provided by P. Romero, University of Lausanne. The short hairpin against control (shCTRL) or UGCG (shUGCG) sequence were insert into the lentiviral vector PLKO.1 purchased from Addgene between AgeI and EcoRI restriction sites. All the gRNAs cloning sequences and primers for cloning are listed in Supplementary Table 1. The following chemical reagents were used in this study: mouse IL-4 (214-14, Peprotech), mouse IL-6 (216-16, Bioconcept), mouse IL-13 (210-13, Peprotech), STF081030 (S7771, SelleckChem), anti-IL-6 Ab (504502, BioLegend), anti-IL-10 Ab (504902, BioLegend), anti-IL-4 Ab (504102, BioLegend), anti-IL-13 Ab (500-P178, Peprotech), anti-Mincle Ab (mabg-mmcl, InvivoGen), anti-CD36 Ab (clone CRF D-2712[58] provided by R. Silverstein at the Medical College of Wisconsin), GW3965 (S2630, SelleckChem), Tunicamycin (T7765, Sigma), and Simvastatin (S6196, Sigma).

Retrovirus preparation and transduction

Phoenix cells plated in a T150 tissue culture flask were transfected with 21 μg of the retroviral construct and 14 μg of pCL-ECO with Turbofect transfection reagent (Thermo Fischer Scientific), according to the manufacturer's protocol. After 24h the medium was changed and the virus was collected at 48 h and 72 h post transfection. Retrovirus was added to BMDM culture medium (20% L929 in DMEM) in presence of Polybrene 8 μg/ml and added to the macrophages at day 3 and day 5 of differentiation. At day 6 transduction efficiency was assessed by Thy1.1 staining.

RNA extraction, RT-PCR and qPCR

RNAs were extracted using Trizol reagent (Life Technologies). Complementary DNA was converted from mRNA using PrimeScript RT Master Mix (Takara Bio) according to manufacturer's instructions. cDNA, primers and Master Mix (TB Green Premix Ex Taq, Takara Bio) were prepared in a volume of 10 ml. Quantitative real-time PCR was performed on a LightCycler 480 Instrument II machine (Roche Life Science). Relative expression was normalized by the expression of *Actb* in each sample. Primer sequences are listed in Supplementary Table 2.

Tumor engraftment, bone marrow transplantation and in vivo treatments

For the oncogene-driven melanoma model, 3-week-old Braf/PTEN mice were treated with 4-hydroxytamoxifen on the skin surface, as described before to induce melanoma formation[59]. For tumor engraftment, $5x10^4$ cells of YUMM1.7, or $1x10^6$ of YUMM1.7-OVA or $2x10^5$ of YUMM1.7 shCTRL and shUGCG tumor cells, $2x10^5$ of B16-OVA and $7x10^5$of MC38-OVA were injected subcutaneously in 50 µl phosphate-buffered saline. Tumor growth were measured every 2–3 days after tumor engraftment or the indicated treatments. For BM transplantation experiment, 7-week-old C56BL/6 recipient mice were irradiated with 9 Gy. Subsequently, 10^7 bone marrow cells from either LPCAT3$^{fl/fl}$ or LysM-Cre LPCAT3$^{fl/fl}$ mice were injected intravenously. Tumor experiments were initiated 7 weeks post bone marrow reconstitution. For *in vivo* treatment, day 7 post engraftment, YUMM1.7-OVA bearing mice were administrated daily with either 10% DMSO or LXR agonist (GW3965) (10 mg per kg of body weight; SelleckChem) by intraperitoneal injection. For CSF1R blockade, anti-CSF1R Ab (CD115-InVivoMab) was injected I.P. at 50mg/kg of body weight of each mouse every three days starting from day -1 from tumor engraftment. All experiments were performed according to Swiss federal regulations and approved by veterinary authority of Canton Vaud. Maximal tumor burden never exceeded the size permitted by the ethical committee ($1cm^3$).

T cell suppression assay

$CD8^+$ T cells were isolated from spleen using negative selection Mojosort kit (BioLegend). Isolated $CD8^+$ T cells were labelled with 5µg/ml of CFSE (Life technology) for 10 minutes at 37°C protected from light. Then, cells were washed, resuspended with medium containing 10 ng/ml of murine IL-2 (Peprotech) and seeded on wells coated with anti-CD3 and anti-CD28 antibodies (2µg/ml) to allow activation in a ratio 2:1 (2-CD8T: 1-BMDM) with BMDM previously treated for 24h with the treatment indicated in figure legends. After 72h, CD8T cells were collected, stained and analysed by flow cytometry.

Tumor digestion, cell isolation and fluorescence-activated cell sorting analysis

Tumors were minced in RPMI with 2% FBS, DNaseI (1 µg/ml, Sigma-Aldrich) and collagenase (1 mg/ml, Sigma-Aldrich), followed by digestion at 37 °C for 50 min. After digestion, the samples were filtered through a 70-µm cell strainer. Leukocytes enrichment was performed by density gradient centrifugation (800g, 30 min) at 25 °C with 40% and 80% percoll (GE Healthcare). Isolated cells were incubated with Fc receptor-blocking anti-CD16/32 (93) antibodies (BioLegend) at 4 °C for 10 min, washed and stained for

surface markers for 30 min on ice. Then, intracellular staining procedure was performed as described[60]. Fluorescence-activated cell sorting (FACS) analyses were performed by using LSRII flow cytometer (BD Biosciences) with BD FACSDiva software (v.8.0.1). Data analysis was performed by using FlowJo. Mature TAMs (mTAMs) were defined as $CD45^+CD3^-Ly6G^-CD11b^+F480^+Ly6C^-$, immature TAMs (iTAMs) were defined as $CD45^+CD3^-Ly6G^-CD11b^+F480^+Ly6C^{int}$. The following antibodies were used: anti-CD45.2, 1:100 (Ali4A2), anti-CD3ε, 1:100 (17A2), anti-Gr1, 1:100 (RB8-6C5), anti-Ly6G, 1:200 (1A8), anti-CD11b, 1:200 (M1/70), anti-Ly6C, 1:2000 (HK1.4), anti-F4/80, 1:100 (BMB), anti- PDL1(CD274), 1:100 (MIH5), anti-MHCII (IAd-IEd), 1:2000 (M5/114.15.2), anti-sXBP1, 1:50 (Q3-695), anti-CD206, 1:100 (MMR), anti-ARG1, 1:100 (A1exF5), and anti-phosphoPERK (Thr980), 1:50 (BS3330R). These antibodies were purchased from BioLegend, BD-Bioscience or Invitrogen.

Fatty acid uptake and lipid content measurement

To determine fatty acid uptake, cells were cultured in RPMI medium containing 0.5 μM of BODIPY 500/510 C12 (Life Technologies) at 37 °C for 15 min and then washed with FACS buffer for surface staining. For detection of lipid content and cholesterol content, after permeabilization and fixation, cells were stained using BODIPY 493/503 (Life Technologies) at a final concentration of 2 μM for measuring lipids or with Filipin III (Sigma) at a final concentration of 20μg/ml for measuring cholesterol content, together with other intracellular proteins.

Electron microscopy

Sorted cells were fixed in 2.5% glutaraldehyde solution (EMS) 1h at room temperature, and directly postfixed with 1% osmium tetroxide (EMS)/1.5% potassium ferrocyanide (Sigma) for 1h at room temperature. After several washes and dehydration in acetone (Sigma), cells were then embedded in Epon resin (Sigma). Sections of 50 nm were prepared on a Leica Ultracut microtome (Leica Mikrosysteme), followed by poststaining with 4% uranyl acetate (Sigma) and Reynolds' lead citrate (Sigma). Images were recorded with a transmission electron microscope Philips CM100 (ThermoFisher Scientific) at an acceleration voltage of 80 kV with a TemCam-F416 digital camera (TVIPS). Analysis and quantification were performed by using ImageJ software. For assessing ER extension, each dot represents the total length of ER compartment assessed by analyzing the length of each selected line of ER in the ROI manager.

RNA-sequencing

The RNA-sequencing (RNA-seq) data was processed using the standard RNA-seq analysis pipeline as reported before[14]. Briefly, read alignment was performed using tophat2 v2.1.0 (parameters "–no-novel-junctions" and "–G" when specifying the genome file), with *Mus musculus* GRCm38.p4 genome version as the reference genome. Read counts were generated using HTseq count, and the differential expression analysis of the counts were performed using the DESeq2 R library. FDR-adjusted p value after Benjamini-Hochberg correction for multiple-testing were used as the statistics to define the differential expression. Genes with FDR-adjusted p value less than 0.05 are considered to be significantly differentially expressed.

Immunoblot analysis

Protein extraction was performed using RIPA lysis buffer (50 mM Tris HCl pH 7.4, 150 mM NaCl, 1% NP-40, 0.5% sodium deoxycholate, 0.1% SDS, 2mM EDTA) supplemented with Complete Protease Inhibitor Cocktail (Roche) and sodium orthovanadate. After incubation on ice for 30 minutes, lysates were centrifugated 15 minutes at 4°C to remove cellular debris. Protein concentration was determined and then subjected for immunoblotting assay. The signal was visualized with Supersignal West Femto max or Supersignal West Pico max chemiluminescent substrate (Thermo Scientific) with a digital imager. The following primary antibodies were used: anti-sXBP1(D2C1F-Cell Signaling), anti-sXBP1 (6195-BioLegend), phospho-Y705 STAT3 (AP0070-Abclonal), STAT3 (A1192-Abclonal), monoclonal anti-bactin (A2228-Sigma), anti-Tubulin (AG-27B-005 Adipogen), anti-UGCG (ab124296-Abcam), anti-PERK (C33E10-Cell Signaling), anti-IRE1 (14C10-Cell Signaling), anti-ATF4 (sc-200, Santa Cruz).

Targeted lipidomic of the ER

The microsomal compartment of the cells was isolated through differential centrifugation as previously described[61]. Briefly, cells were collected in PBS and after centrifugation were resuspended with ice-cold 250-STMDPS Buffer (250 mM sucrose, 50 mM Tris-HCl (pH 7.4), 5 mM MgCl2) in presence of protease inhibitors and homogenized for a minimum of 5 min using a tight-fitting pestle. The solution was transferred in a tube and centrifuge at 800g for 15’ at 4C. Supernatant was transferred in a new tube and pellets were resuspended with 5 volumes of 250-STMDPS Buffer and re-homogenize for 10 min in homogenizers. Then the solution was centrifuged at 800g for 15 min. Supernatants from both centrifugation steps were then collected and subjected for centrifuge at 6,000g for 15 min to pellet the mitochondria. The remaining supernatants were subjected to ultracentrifuge for 1 h at 100,000g in a swing-bucket ultracentrifuge to collect pellets for microsomal (ER) fraction. Microsomal pellets were then re-suspended with Methanol/Water (80:20) and then 25 µL of the resulting solution was extracted with 125 µL of Buthanol:MeOH (1:1) by vortexing. The extracts were centrifuged for 15 minutes at 4000 g at 4°C (Hermle, Gosheim, Germany) and the resulting supernatant was collected and transferred to LC-MS vials for injection. Cell extracts were analyzed by Hydrophilic Interaction Liquid Chromatography coupled to tandem mass spectrometry (HILIC - MS/MS) in both positive and negative ionization modes using a Q-TRAP 6500 plus LC-MS/MS instrument (Sciex, Framingham, MA, USA). Lipid separation was carried out on an Acquity BEH Amide, 1.7 µm, 100 mm × 2.1 mm I.D. column (Waters, Massachusetts, US). Mobile phase was composed of A = 10 mM ammonium acetate in Acetonitrile:H_2O (95:5) and B = 10 mM ammonium acetate in Acetonitrile:H_2O (50:50). The linear gradient elution from 0.1% to 20% B was applied for 2 minutes, then from 20% to 80% B for 3 minutes, followed by 3 minutes of re-equilibration to the initial chromatographic conditions. The flow rate was 600 µL/min, column temperature 45 °C and sample injection volume 2 µl. Optimized ESI Ion Drive Turbo V source parameters were set as follows: Ion Spray (IS) voltage 5500 V in positive mode and - 4500 V in negative mode, curtain gas 35 psi, nebulizer gas (GS1) 50 psi, auxiliary gas (GS2) 60 psi, source temperature 550°C. Nitrogen was used as the nebulizer and collision gas. Optimized compound-dependent parameters were used for data

acquisition in scheduled multiple reaction monitoring (s**MRM**) mode. Pooled quality control samples (representative of the entire sample set) were analyzed periodically (every 4 to 5 samples) throughout the overall analytical run, in order to assess the quality of the data, correct the signal intensity drift and remove the peaks with poor reproducibility (CV > 30%). In addition, a series of diluted quality controls (dQC) were prepared by dilution with buthanol:methanol: 100% QC, 50%QC, 25%QC, 12.5%QC and 6.25%QC and analyzed at the beginning and at the end of the sample batch. This QC dilution series served as a linearity filter to remove the features which don't respond linearly (correlation with dilution factor is < 0.65). Raw LC-MS/MS data was processed using the MultiQuant Software (version 3.0.3, Sciex technologies). Relative quantification of metabolites was based on EIC (Extracted Ion Chromatogram) areas for the monitored MRM transitions. The obtained tables (containing peak areas of detected metabolites across all samples) were exported to "R" software http://cran.r-project.org/ where the signal intensity drift correction was done within the LOWESS/Spline normalization program[62] followed by noise filtering (CV (QC features) > 30%) and visual inspection of linear response.

Measurement of β-glucosylceramide

Serum and TIF (Tumor Interstitial Fluid) were isolated from YUMM1.7-tumor bearing mice at day 14 after engraftement or from Braf/Pten inducible melanoma bearing mice at week 7 post tumor induction. Conditioned medium (CM) from shCTRL or shUGCG YUMM1.7 cells was isolated from cells seeded at 70% confluency and kept in culture for 24h. Samples were completed to 20 µL with water and extracted and homogenized by the addition of 80 µL of Methanol spiked with the isotopic labelled internal standards (Spa (d17:0), Cer (d18:1/16:0)-d9, Cer (d18:1/18:0)-d7, Cer (d18:1/24:0)-d7 and Cer (d18:1/24:1)-d7)), respectively. The resulting supernatant were collected and analysed by LC-MS/MS. Extracted samples were analysed by Reversed Phase Liquid Chromatography coupled to tandem mass spectrometry (RPLC - MS/MS) in positive ionization modes using a 6495 triple quadrupole system (QqQ) interfaced with 1290 UHPLC system (Agilent Technologies) adapted from Checa et al.[63].

Single-Cell RNA-seq Data Processing

The processed single-cell gene expression datasets for different tumors including human colorectal cancer[25], lung tumors[26, 27], and mouse sarcoma[28] were collected from Gene Expression Omnibus (https://www.ncbi.nlm.nih.gov/geo/) and single cell portal (https://singlecell.broadinstitute.org/) using their public accessions. The lung tumor subtypes were defined according to sample origins (tumor subtype and disease type)[26]. The M1 and M2 macrophages were defined by comparing the average expression of M1/M2 signatures[25], except for the mouse sarcoma dataset in which both M1 and M2 had been labeled. Those cells with the average expression of M1 signatures larger than that of M2 signatures were classified as the M1 like macrophages, and others were classified as the M2 like macrophages. The ER stress score for each cell was defined as the average expression of ER stress response genes collected from https://www.gsea-msigdb.org/gsea/msigdb/cards/GO_RESPONSE_TO_ENDOPLASMIC_RETICULUM_STRESS. For mouse sarcoma, the ER stress-related genes were converted to human gene symbols using biomaRt[64]. One-sided t-test was used to comparing the ER stress scores between M1 and M2 like macrophages.

Measurement of cytokines and lipids

Cytokine levels (IL-4, IL-10, IL-13 and IL-6) in CM from YUMM1.7 or MEF cells were measured using the kit LEGENDplex murine Th Cytokine panel 12-plex, according to manufacturer's instruction. Samples were acquired on LSRII and analysed using LEGENDplex software (BioLegend). Cholesterol and fatty acid in CM and CM without lipids were measured by using Total Cholesterol and Cholesteryl Ester Colorimetric/Fluorometric Assay Kit (Biovision) and Free Fatty Acid Quantification Colorimetric/Fluorometric Kit (Biovision) respectively. Quantification was performed following manufacturer's instructions.

RNA extraction, RT-PCR and qPCR

RNAs were extracted using TRIzol reagent (Life Technologies). Complementary DNA was converted from mRNA using PrimeScript RT Master Mix (Takara Bio) according to manufacturer's instructions. cDNA, primers and Master Mix (TB Green Premix Ex Taq, Takara Bio) were prepared in a volume of 10 ml. Quantitative real-time PCR was performed on a LightCycler 480 Instrument II machine (Roche Life Science). Relative expression was normalized by the expression of Actin in each sample.

Proximity Ligation assay

BMDMs from indicated treatment conditions were fixed with 4% paraformaldehyde at 37°C for 15 mins and permeabilized with 0.2% Triton in PBS at RT for another 15 minutes. Duolink® In Situ Red Starter Kit Mouse/Rabbit was used according to manufacturer's instructions. Anti-STAT3 (124H6) Mouse mAb and anti-IRE1 rabbit polyclonal Ab (37073) were used as primary antibodies. Images were acquired with confocal microscope Zeiss LSM800 and quantified using ImageJ software.

Data analysis and statistics

Biological replicates and presentation in each figure are shown as mean ± s.e.m. as mentioned in the figure legends. Statistical significance was determined by using two-tailed, unpaired, Student's *t*-test, paired-t test, ordinary one-way ANOVA corrected for Sidak's or Tukey's multiple comparison test, or multiple repeated one-way ANOVA with Bonferroni's multiple comparison as mentioned in the figure legends. No statistical methods were used to pre-determine sample size but our sample sizes are similar to those reported in previous publications[14]. Data distribution was assumed to be normal but this was not formally tested. Unless when restricted by the genotype, animals and cell plates were randomly assigned to experimental conditions. Data collection and analysis were not performed blind to the conditions of the experiments. No data exclusion was performed.

Extended Data

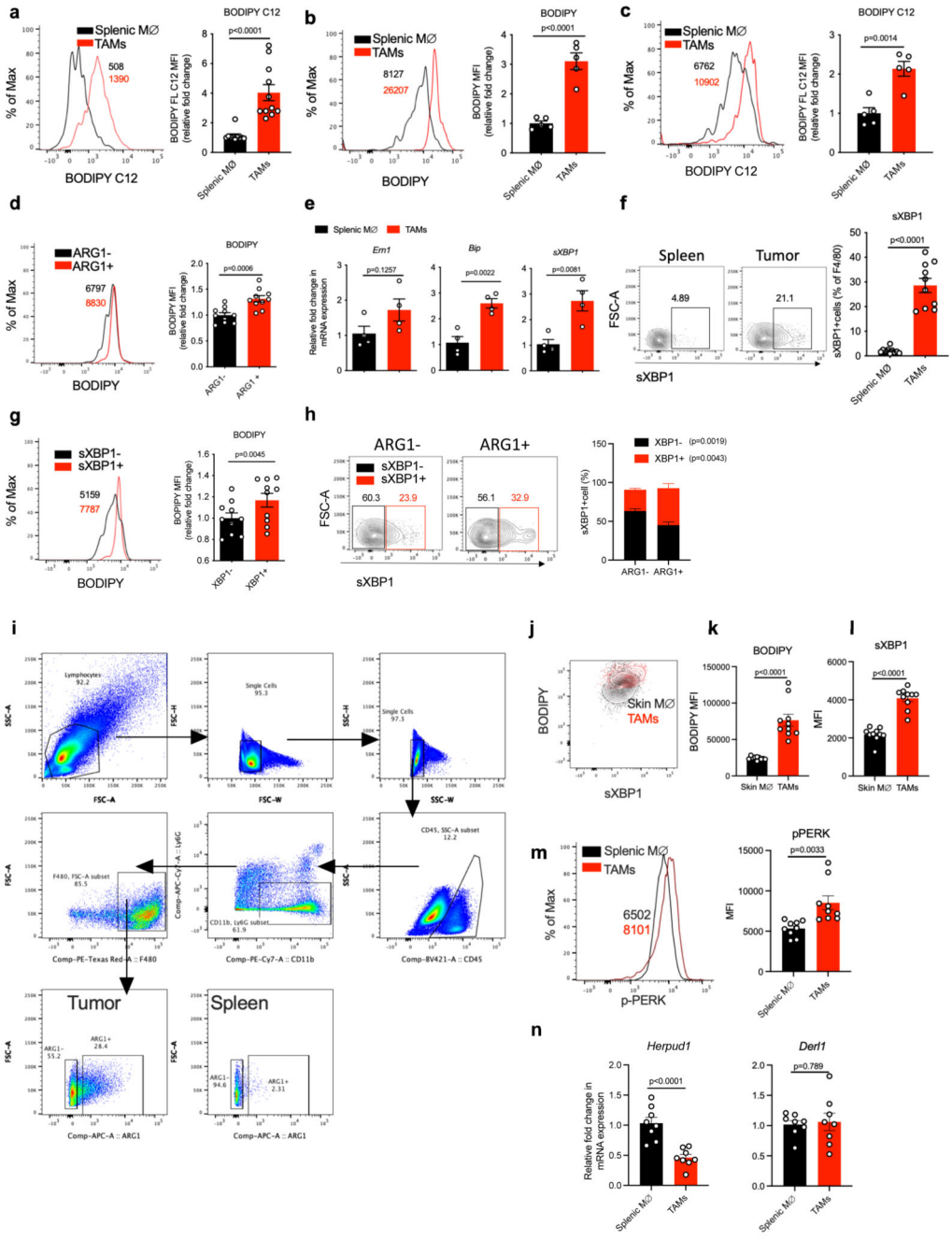

Extended Data Fig. 1. TAMs display high lipid content and ER stress responses in the inducible Braf/Pten melanoma model

a, Representative histogram (left) and quantitative plot (right) of BODIPY C12 staining in splenic macrophages (n=10) or tumor-associated macrophages (TAMs) (n=11) from YUMM1.7 melanoma bearing mice. Data are pooled from two independent experiment. **b-h,** Analysis of Braf/Pten tumor-bearing mice seven weeks after tamoxifen administration. **b-c**, Representative histogram (left) and quantitative plot (right) of BODIPY staining (**b**) and

Europe PMC Funders Author Manuscripts

BODIPY C12 staining (**c**) in splenic macrophages or TAMs isolated from Braf/Pten tumor-bearing mice (*n*=5 per group). **d**, Representative histogram (left) and quantitative plots (right) of BODIPY staining in TAMs gated based on ARG1 expression (*n*=10 per group). **e**, qPCR analysis of mRNA expression of the indicated genes in splenic macrophages and TAMs isolated from Braf/Pten tumor-bearing mice (*n*=4 per group). **f**, Representative histogram (left) and quantitative plot of the abundance (right) of $sXBP1^+$ subset among splenic macrophages and TAMs in Braf/Pten tumor-bearing mice (*n*=10 per group). **g,** Representative histogram (left) and quantitative plot (right) of BODIPY staining in TAMs gated based on sXBP1 expression (*n*=10 per group). **h**, Representative histogram (left) and quantitative plot of the abundance (right) of $sXBP1^+$ cells among $ARG1^+$ and $ARG1^-$ TAMs (*n*=10 per group). **i**, Gating strategy applied to define ARG1+ macrophages from spleen and tumor of YUMM1.7 tumor-bearing mice. **j-l,** Representative histogram (**j**) and quantitative plot of BODIPY staining (**k**) or sXBP1 (**l**) in skin-resident macrophages or TAMs from Braf/Pten tumor-bearing mice (*n*=10 per group). **m,** Representative histogram (left) and quantitative plot (right) of pPERK staining in splenic macrophages or tumor-associated macrophages (TAMs) (*n*=9 per group) of YUMM1.7 melanoma bearing mice. Data are pooled from two independent experiments. **n**, qRT-PCR of the indicated genes from sorted splenic macrophages and TAMs (*n*=8 per group) isolated from YUMM1.7 tumor-bearing mice. Data are representative of two independent experiments (**b, c, e**). Data are pooled from two independent experiment (**a**, **d, f-h, j-n**). Each symbol represents one individual. All data are mean ± s.e.m and were analysed by two-tailed, unpaired Student's t-test or paired t-test (**d**, **g**, **h**).

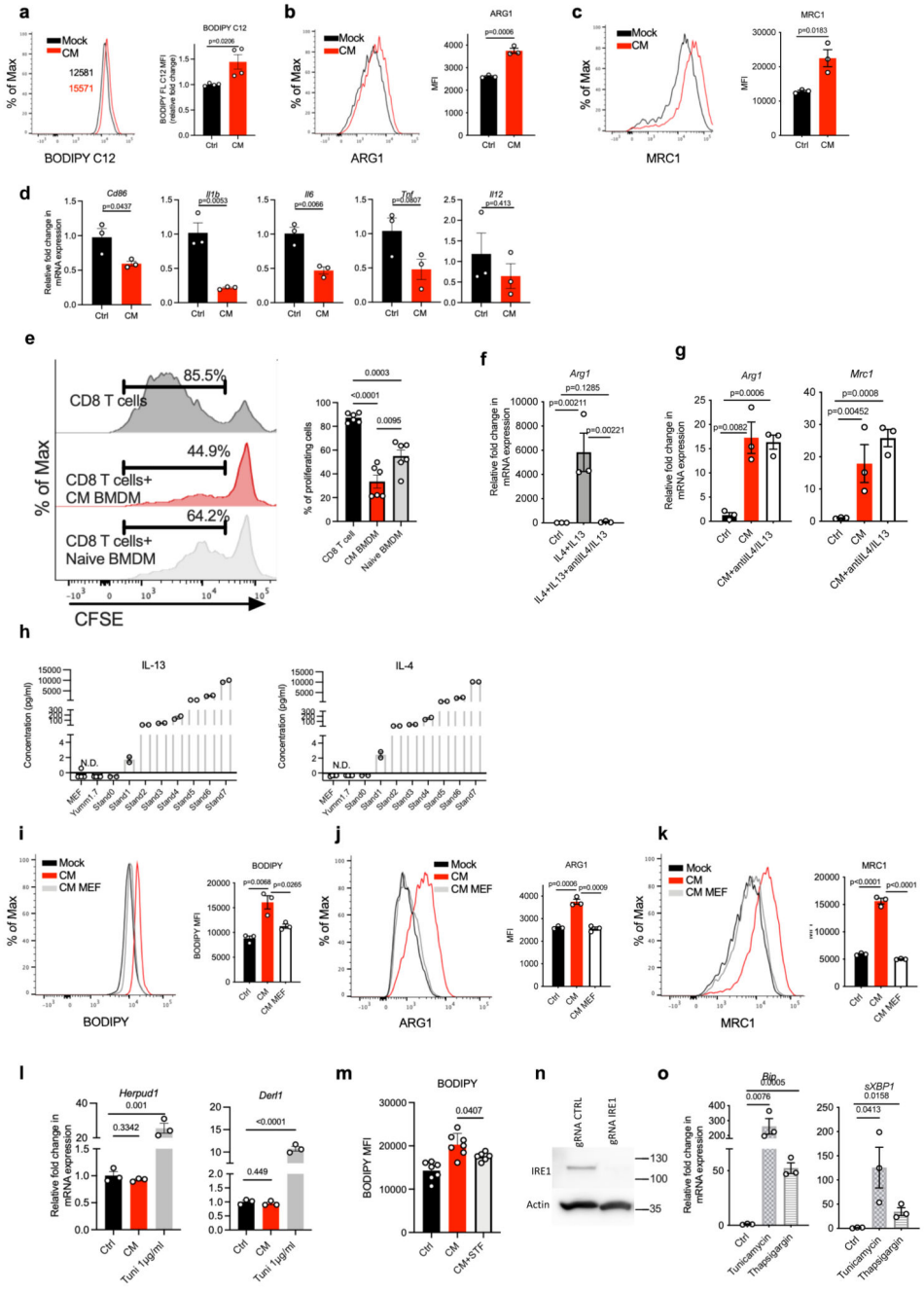

Extended Data Fig. 2. Tumor cells reinforce pro-tumorigenic polarization in macrophages via an IL-4/IL-13 independent manner

a, Representative histogram (left) and quantitative plot (right) of BODIPY FL C12 staining in BMDM cultured in DMEM (Ctrl) or YUMM1.7 CM (n=4 per group). Data are representative of two independent experiments. **b-c**, Representative histogram (left) and quantitative plot (right) of ARG1 (**b**) and MRC1 (**c**) expression in BMDMs cultured in DMEM or CM (n=3 per group). Data are representative of three independent experiments. **d**, qPCR analysis of mRNA expression of the indicated genes in BMDMs cultured in DMEM

Europe PMC Funders Author Manuscripts

Europe PMC Funders Author Manuscripts

or CM for 18h (*n*=3 per group). Data are representative of three independent experiments. **e,** Proliferation of CFSE-labelled T cells activated with anti-CD3 and anti-CD28 alone or in co-culture with BMDM Naïve or previously exposed to CM in a ratio 2:1 (*n*=6). Data are pooled of two independent experiments. **f**, qPCR analysis of ARG1 mRNA expression in BMDMs treated with IL-4 and IL-13 (10ng/ml) in the absence or presence of 0.25μg/ml anti-IL-4 and 0.25μg/ml anti-IL-13 neutralizing antibodies for 18h (*n*=3 per group). **g,** qPCR analysis of mRNA expression of indicated genes in BMDMs treated with CM in the absence or presence of 0.25μg/ml anti-IL-4 and 0.25μg/ml anti-IL-13 neutralizing antibody for 18h (*n*=3 per group). Data are representative results of three independent experiments. **h,** Multiplex cytokine array was used to determine the concentration of IL13 (left) and IL4 (right) in CM from YUMM1.7 and MEF cells. Stand0 to Stand7 show the increased concentration detected by the standard provided by the kit (*n*=4). Data are representative of two independent experiments. **i-k,** Representative histogram (left) and quantitative plot (right) of BODIPY staining (**i**), and protein expression of ARG1 (**j**), and MRC1 (**k**) in BMDMs stimulated with regular culture medium (Ctrl) or CM from YUMM1.7 (CM) or MEF (CM MEF) (*n*= 3 per group). Data are representative results of three independent experiments. **l**, qPCR analysis of indicated genes in BMDMs exposed to CM or Tunicamycin for 18h (*n*=3 per group). Data are representative results of three independent experiments. **m,** Quantification of BODIPY staining in BMDMs treated with CM in the absence or presence of 50μM STF083010; Ctrl (*n*=7), CM (*n*=7), CM-STF (*n*=6). Data are pooled from three independent experiments. **n,** Immunoblots of indicated proteins in BMDM transduced with retrovirus expressing scramble or IRE1-targeting gRNAs. **o,** qPCR analysis of BIP and sXBP1 mRNA expression in BMDMs treated with lμγ/ml of Tunicamycin, 1μM thapsigargin and CM for 16h (*n*=3 per group). Data are representative results of three independent experiments. Data are mean ± s.e.m. were analysed by two-tailed, unpaired Student’s t-test or one-way ANOVA with Tukey’s multiple comparison test (**e**).

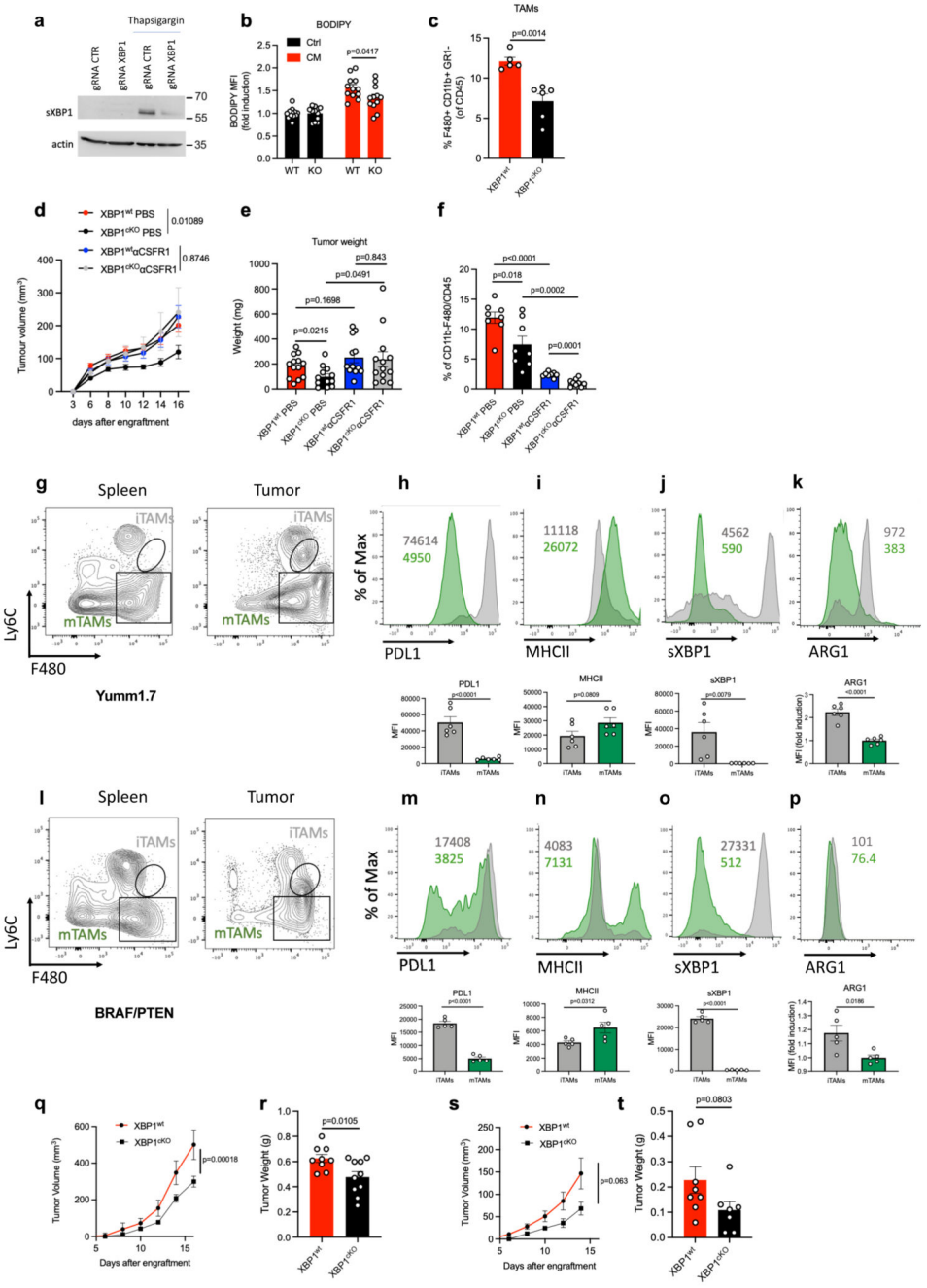

Extended Data Fig. 3. XBP1 supports pro-tumorigenic polarization in response to cancer-derived stimuli

a, Immunoblots of indicated proteins in control or XBP1-deficient BMDMs stimulated with or without 1 μM thapsigargin for 6h. Data are representative results of two independent experiments. **b,** Quantification of BODIPY staining in BMDMs generated from WT ($XBP1^{wt}$) or KO ($XBP1^{cKO}$) mice cultured stimulated with regular culture medium (Ctrl) or YUMM1.7 CM (n=12 per group). Data are pooled from three independent experiments. **c,** Percentages of TAMs ($F4/80^{+}$ $CD11b^{+}$ $Gr1^{-}$) among $CD45^{+}$ cells in melanomas from

Europe PMC Funders Author Manuscripts

tumor-bearing XBP1^{wt} (n=5) and XBP1^{cKO} mice (n=6). Data are representative results of three independent experiments. **d-e,** Tumor growth (**d**) and tumor weight (**e**) of YUMM1.7-OVA melanoma from WT and XBP1^{cKO} mice treated with PBS or with anti-CSF1R as indicated in the methods; XBP1^{wt} PBS (n=13), XBP1^{cKO} PBS mice (n=12), XBP1^{wt} αCSF1R (n=12), XBP1^{cKO} αCSF1R (n=13). Data are pooled from three independent experiments. **f**, percentages of TAMs (F4/80+ cells gated on CD11b+Gr1-) among CD45+ cells in the experiment showed in **d-e** (n=8 per group for XBP1^{wt} PBS, XBP1^{cKO} PBS, XBP1^{wt} αCSF1R; n=9 for XBP1^{cKO} αCSF1R). Data are pooled from two independent experiments. **g,** Representative plots of iTAMs and mTAMs populations in tumor and spleen of YUMM1.7 tumor-bearing. **h-k,** Representative histograms (up) and quantitative plots (down) of PDL1 (**h**), MHCII (**i**), sXBP1 (**j**) and ARG1 (**k**) expression in iTAMs and mTAMs from YUMM1.7 tumor-bearing mice (n=6). Data are pooled from two independent experiments. **l,** Representative plots of iTAMs and mTAMs populations in tumor and spleen of Braf/Pten melanoma-bearing mice. **m-p,** Representative histograms (up) and quantitative plots (down) of PDL1 (**m**), MHCII (**n**), sXBP1 (**o**) and ARG1 (**p**) expression in iTAMs and mTAMs from Braf/Pten melanoma-bearing mice (n=5). Data are representative of two independent experiments. Each symbol represents one individual. **q-t**, Tumor growth (**q**) and tumor weight (**r**) of B16-OVA melanoma and tumor growth (**s**) and tumor weight (**t**) of MC38-OVA colon adenocarcinoma in XBP1^{wt} (n=9 for B16-OVA and n=8 for MC38-OVA) or XBP1^{cKO} (n=10 for B16-OVA and n=7 for MC38-OVA) mice. Data are pooled from two independent experiments. Data are mean ± s.e.m. were analysed by two-tailed, unpaired Student’s t-test.

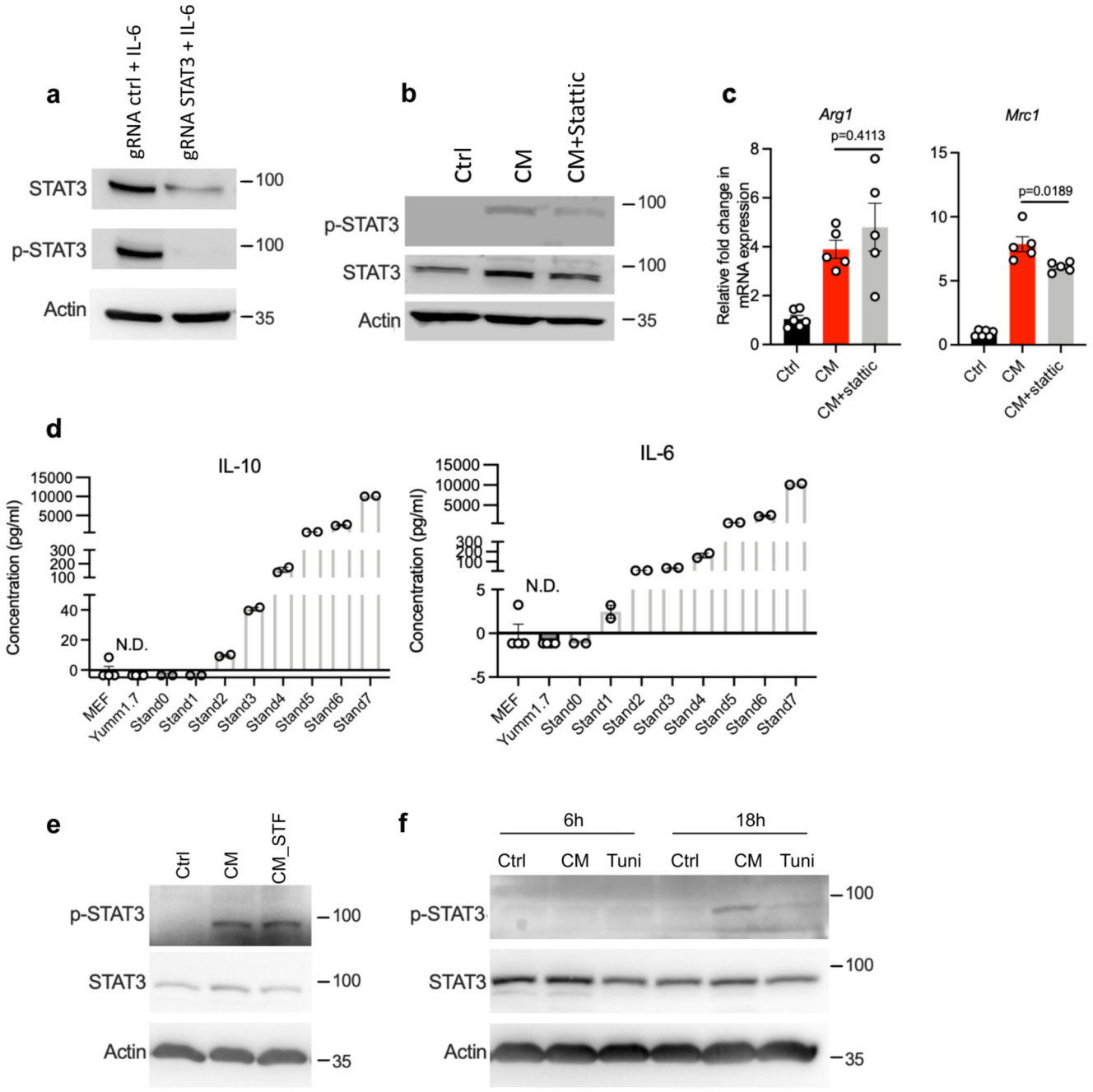

Extended Data Fig. 4. STAT3 is required for CM-induced pro-tumorigenic polarization

a, Immunoblots of indicated proteins in BMDMs expressing scramble or STAT3-targeting gRNAs treated with 10ng/ml IL-6 for 6h. Data are representative results of two independent experiments. **b,c,** Immunoblots of indicated proteins (**b**) and qPCR analysis of mRNA expression of indicated genes (**c**) in BMDMs treated with CM in the presence of vehicle (CM) or 10μM Stattic (CM+Stattic) (n= 6 for Ctrl and n=5 for CM and CM+Stattic). Data are representative results of three independent experiments. **d,** Multiplex cytokine array was used to determine the concentration of IL-10 (left) and IL-6 (right) in CM from YUMM1.7

and MEF cells. Stand0 to Stand7 show the increased concentration detected by the standard provided by the kit (n=4). Data are representative results of two independent experiments. **e**, Immunoblot of indicated proteins in BMDMs treated with control media (Ctrl), cancer cell conditioned media (CM) or CM plus 50μM STF081030 for 18h. Data are representative of two independent experiments. **f**, Immunoblot of BMDMs treated with control vehicle (Ctrl), cancer cell conditioned media (CM) or tunicamycin (1μg/ml; Tuni.) for the indicated time points. Data are representative of two independent experiments. All data are mean ± s.e.m and were analysed by two-tailed, unpaired Student's t-test.

Europe PMC Funders Author Manuscripts

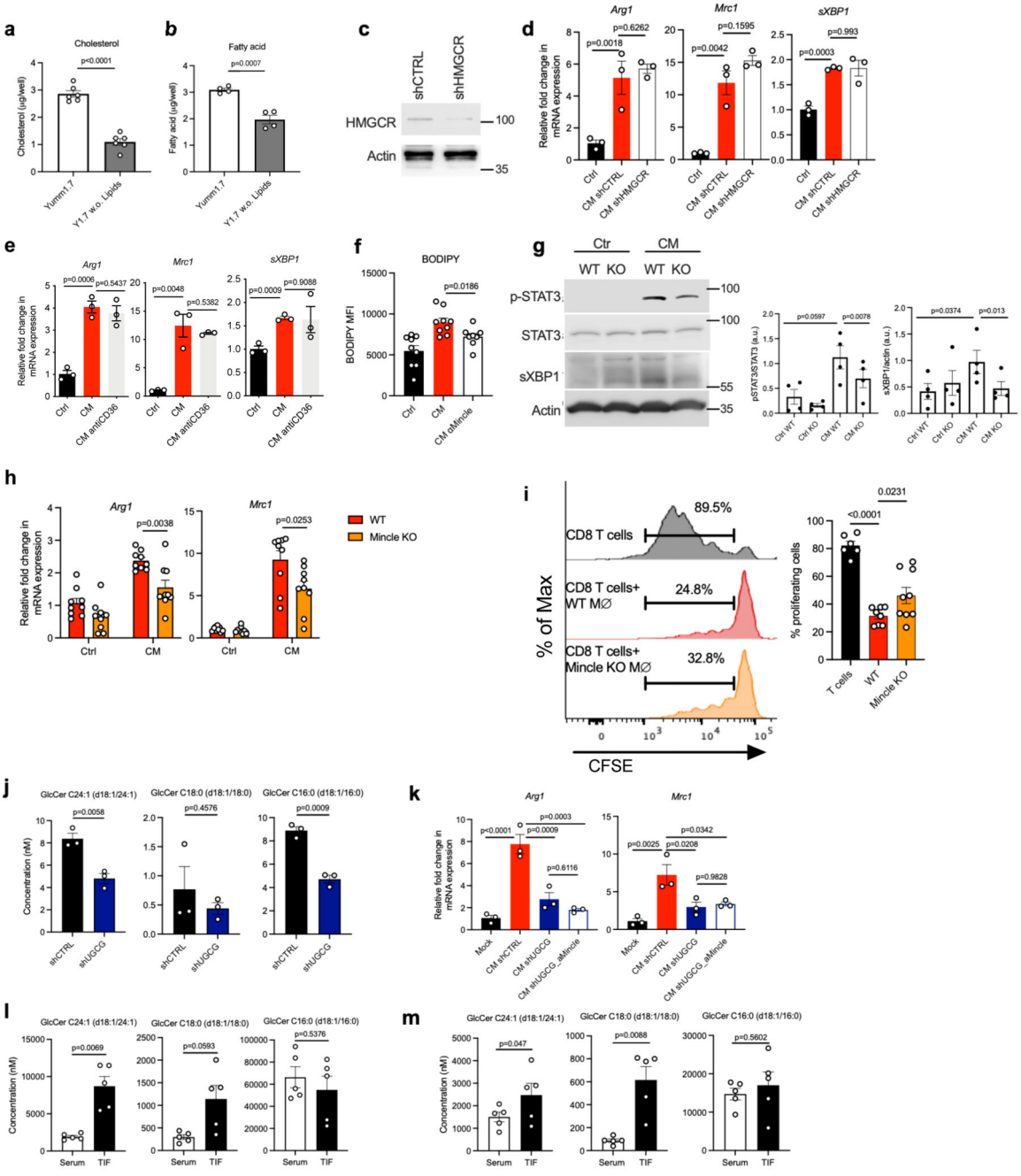

Extended Data Fig. 5. β-glucosylceramide, rather than cholesterol, is released by tumor cells to mediate the pro-tumorigenic polarization in macrophages

a,b, Quantification results of Cholesterol (**a**) (n=6 per group) and fatty acids (**b**) (n=4 per group) on YUMM1.7 CM prior (Yumm1.7) and after treatment with lipid removal reagent (Y1.7 w.o. Lipids). Data are pooled from two independent experiments. **c**, Immunoblot of YUMM1.7 cells stably transduced with lentivirus expressing short hairpin RNA against scramble or HMGCR sequence. **d,** qPCR analysis of indicated genes in BMDMs exposed to CM isolated from YUMM1.7 shCTRL or from YUMM1.7 shHMGCR (n=3). Data are

Europe PMC Funders Author Manuscripts

representative of three independent experiments**. e,** qPCR analysis of mRNA expression of indicated genes in BMDMs treated with CM in the absence or presence of 1μg/ml α-CD36 antibody (*n*= 3 per group). Data are representative results of two independent experiments. **f,** Quantification of BODIPY staining in BMDM cultured with regular culture medium (Ctrl) or with YUMM1.7 CM in the absence or presence of 5μg/ml α-Mincle antibody; Ctrl (*n*=9), CM (*n*=9), CMα-Mincle (*n*=8). Data are pooled from three independent experiments. **g-h**, Immunoblot and quantification of the indicated proteins (**g**) (*n*=4 per group) and qPCR analysis of mRNA expression of ARG1 and MRC1 (**h**) of WT or Mincle-KO BMDMs exposed to regular culture medium (Ctrl) or or with YUMM1.7 CM for 18h (*n*=9 per group). Data are pooled from three independent experiments. **i,** Proliferation of CFSE-labelled T cells activated with anti-CD3 and anti-CD28 alone or co-cultured with WT or Mincle-KO BMDMs previously treated with CM in a ratio 2:1 for 72h; T cells (*n*=6), WT (*n*=8), KO (*n*=9). Data are pooled from three independent experiments. **j,** Quantification result of indicated β-glucosylceramide levels from CM derived from YUMM1.7 shCTRL and YUMM1.7 shUGCG cells (*n*=3 per group). **k,** qPCR analysis of the indicated genes in BMDMs treated with Ctrl or CM derived from YUMM1.7 shCTRL and YUMM1.7 shUGCG cells alone or in presence of αMincle antibody (5μg/ml) (*n*=3). Data are representative of two independent experiments. **l-m,** Quantification result of indicated β-glucosylceramide levels in serum and tumor interstitital fluid (TIF) isolated from YUMM1.7 melanoma-bearing mice (**l**) or Braf/Pten melanoma-bearing mice (**m**) (*n*=5 per group). All data are mean ± s.e.m and were analysed by two-tailed, unpaired Student's t-test (**a-f**), paired Student's t-test (**g, j, l-m**), one-way ANOVA with Sidak's multiple comparison test (**i**), one-way ANOVA with Tukey's multiple comparison test (**k**).

Europe PMC Funders Author Manuscripts

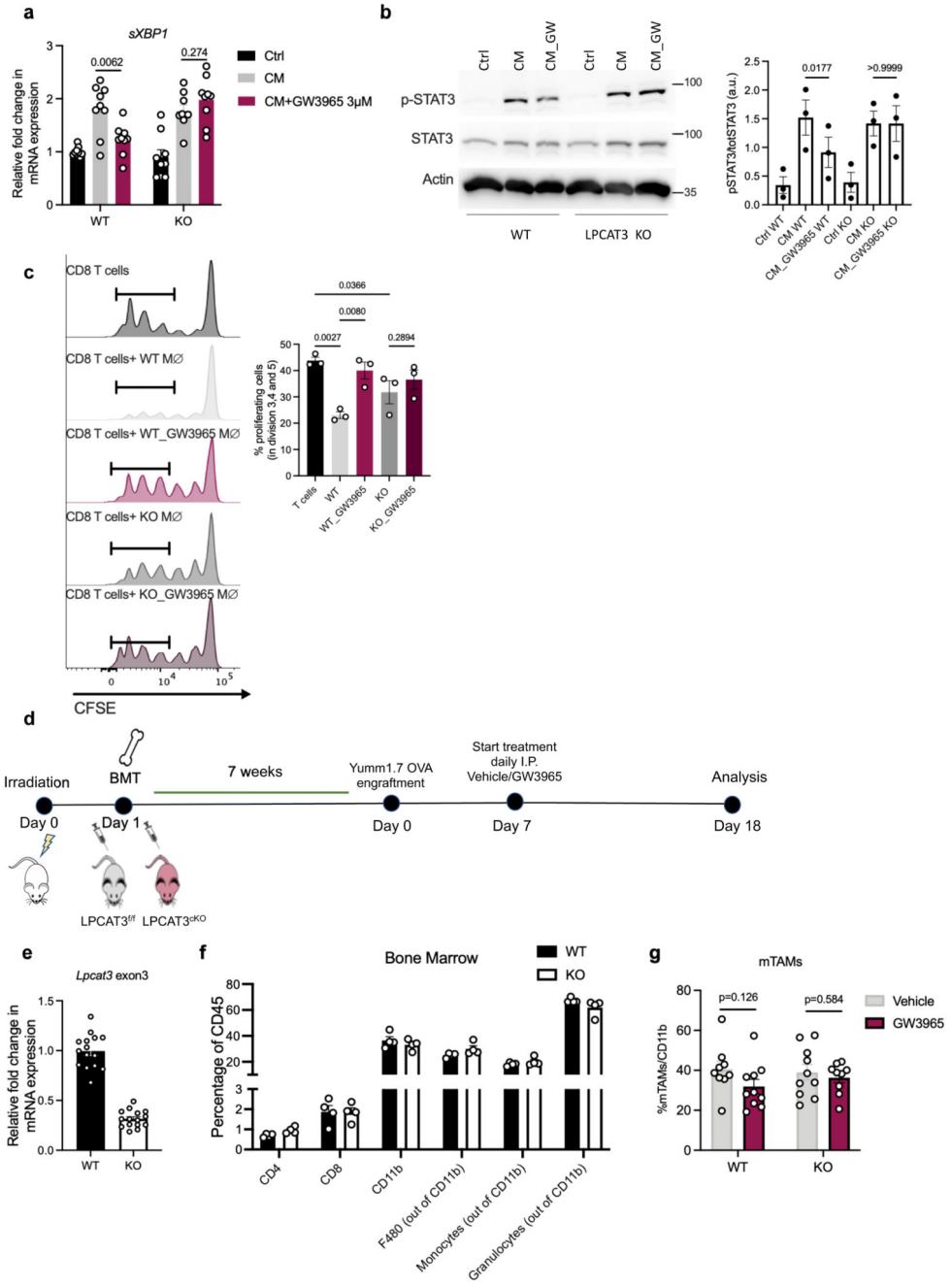

Extended Data Fig. 6. Macrophage-specific ablation of LPCAT3 abolishes GW3965 anti-tumor responses.

a-b, qPCR analysis of mRNA expression of sXBP1 (**a**) and immunoblot and quantification (**b**) of indicated proteins in WT or LPCAT3-KO BMDMs exposed to regular culture medium (Ctrl) and YUMM1.7 CM in absence or presence of 3μM GW3965 ($n = 9$ per group for qPCR and n=3 per group for immunoblots). Data are pooled from three independent experiments **c**, Proliferation of CFSE-labelled T cells activated with anti-CD3 and anti-CD28 alone or co-cultured with WT or LPCAT3-KO BMDMs previously treated

with YUMM1.7 CM in the absence or presence of GW3965 in a ratio 2:1 for 72h (*n* = 3 per group). Data are representative of three independent experiments. **d,** Illustration of experimental design for bone marrow transplantation. **e,** qPCR analysis of exon 3 of LPCAT3 gene in LPCAT3$^{fl/fl}$ (WT) and LysM-Cre LPCAT3$^{fl/fl}$ (KO) mice (*n*=15). **f,** Bone marrow was isolated from WT and KO chimeric tumor-bearing mice and the abundance of indicated immune cells was measured by flow cytometry (*n*=4). **g,** Percentage of mTAMs among CD11b^{+} tumor-infiltrating myeloid cells from YUMM1.7-OVA melanoma treated with either control vehicle or GW3965 in mice transplanted with BM cells from LPCAT3$^{fl/fl}$ (WT) and LysM-Cre LPCAT3$^{fl/fl}$ (KO) mice (WT+Vehicle: *n*=9; WT+GW3965: *n*=10; KO+Vehicle: *n*=10; KO+GW3965: *n*=9). Data are pooled from two independent experiments. Each symbol represents one individual. All data are mean ± s.e.m and were analysed by two-tailed, unpaired Student's t-test (**a, e-g**), RM one-way ANOVA with Bonferroni's multiple comparison test (**b**), and ordinary one-way ANOVA with Tukey's multiple comparison test (**c**).

Supplementary Material

Refer to Web version on PubMed Central for supplementary material.

Acknowledgments

We thank Laurie Glimcher and Gokhan Hotamisligil for providing *XBP1*$^{flox/flox}$ mice and David Sancho for providing Mincle-deficient bone marrows. We thank Takao Shimizu and Jun-ichi Miyazaki for providing LPCAT3-pCNX2 plasmid. P.-C.H. is funded by the Swiss Institute for Experiment Cancer Research (ISREC 26075483), European Research Council Staring Grant (802773-MitoGuide), SNSF project grants (31003A_163204 and 31003A_182470), UNIL Interdisciplinary Grant, the Cancer Research Institute (CLIP investigator award and Lloyd J. Old STAR award) and Ludwig Cancer Research. J.L. is supported by NIH R01CA1932556. P.P. is supported by the New York University Abu Dhabi Research Enhancement Fund Swedish Research Council (Vetenskapsrådet), Swedish Cancer Society (Cancerfonden). D.M. is supported by French government grants managed by the French National Research Agency under the references ANR-11-LABX-0021, ANR-15-IDEX-0003 and ANR-19-CE14-0020. S.C-C.H. is supported by Cancer Research Institute CLIP Investigator Award, the VeloSano Pilot Award, the Case Comprehensive Cancer Center American Cancer Society Pilot Grants, and the Cleveland Digestive Diseases Research Core Center Pilot Grant (IRG-91-022-19, IRG-16-186-21, 1P30DK097948). L.R. is supported by Immunology T32 Training Program (AI089474). J.I. is supported by SNSF R'Equip 316030_183377. F.M. is supported by Swiss Cancer league KFS-4230-08-2017.

Data availability

RNA-seq result is available in the Gene Expression Omnibus database under accession code (GSE166735). Other data are available from the corresponding author upon request.

References

1. Lopez-Yrigoyen M, Cassetta L, Pollard JW. Macrophage targeting in cancer. Ann N Y Acad Sci. 2020; doi: 10.1111/nyas.14377
2. Anfray C, Ummarino A, Andon FT, Allavena P. Current Strategies to Target Tumor-Associated-Macrophages to Improve Anti-Tumor Immune Responses. Cells. 2019; 9 doi: 10.3390/cells9010046
3. Loke P, Allison JP. PD-L1 and PD-L2 are differentially regulated by Th1 and Th2 cells. Proc Natl Acad Sci U S A. 2003; 100 :5336–5341. [PubMed: 12697896]
4. Laoui D, et al. Tumor hypoxia does not drive differentiation of tumor-associated macrophages but rather fine-tunes the M2-like macrophage population. Cancer Res. 2014; 74 :24–30. [PubMed: 24220244]

5. Qian BZ, Pollard JW. Macrophage diversity enhances tumor progression and metastasis. Cell. 2010; 141 :39–51. [PubMed: 20371344]
6. Wenes M, et al. Macrophage Metabolism Controls Tumor Blood Vessel Morphogenesis and Metastasis. Cell Metab. 2016; 24 :701–715. [PubMed: 27773694]
7. Casazza A, et al. Impeding macrophage entry into hypoxic tumor areas by Sema3A/Nrp1 signaling blockade inhibits angiogenesis and restores antitumor immunity. Cancer Cell. 2013; 24 :695–709. [PubMed: 24332039]
8. Pyonteck SM, et al. CSF-1R inhibition alters macrophage polarization and blocks glioma progression. Nat Med. 2013; 19 :1264–1272. [PubMed: 24056773]
9. Topper MJ, et al. Epigenetic Therapy Ties MYC Depletion to Reversing Immune Evasion and Treating Lung Cancer. Cell. 2017; 171 :1284–1300. e1221 [PubMed: 29195073]
10. Liu Y, et al. Tumor-Repopulating Cells Induce PD-1 Expression in CD8(+) T Cells by Transferring Kynurenine and AhR Activation. Cancer Cell. 2018; 33 :480–494. e487 [PubMed: 29533786]
11. Li X, et al. Navigating metabolic pathways to enhance antitumour immunity and immunotherapy. Nat Rev Clin Oncol. 2019; 16 :425–441. [PubMed: 30914826]
12. Vriens K, et al. Evidence for an alternative fatty acid desaturation pathway increasing cancer plasticity. Nature. 2019; 566 :403–406. [PubMed: 30728499]
13. Chen M, et al. An aberrant SREBP-dependent lipogenic program promotes metastatic prostate cancer. Nat Genet. 2018; 50 :206–218. [PubMed: 29335545]
14. Wang H, et al. CD36-mediated metabolic adaptation supports regulatory T cell survival and function in tumors. Nat Immunol. 2020; 21 :298–308. [PubMed: 32066953]
15. Herber DL, et al. Lipid accumulation and dendritic cell dysfunction in cancer. Nat Med. 2010; 16 :880–886. [PubMed: 20622859]
16. Veglia F, et al. Fatty acid transport protein 2 reprograms neutrophils in cancer. Nature. 2019; 569 :73–78. [PubMed: 30996346]
17. Di Conza G, Ho PC. ER Stress Responses: An Emerging Modulator for Innate Immunity. Cells. 2020; 9 doi: 10.3390/cells9030695
18. Chen X, Cubillos-Ruiz JR. Endoplasmic reticulum stress signals in the tumour and its microenvironment. Nat Rev Cancer. 2020; doi: 10.1038/s41568-020-00312-2
19. Song M, et al. IRE1alpha-XBP1 controls T cell function in ovarian cancer by regulating mitochondrial activity. Nature. 2018; 562 :423–428. [PubMed: 30305738]
20. Ma X, et al. Cholesterol Induces CD8(+) T Cell Exhaustion in the Tumor Microenvironment. Cell Metab. 2019; 30 :143–156. e145 [PubMed: 31031094]
21. Cubillos-Ruiz JR, et al. ER Stress Sensor XBP1 Controls Anti-tumor Immunity by Disrupting Dendritic Cell Homeostasis. Cell. 2015; 161 :1527–1538. [PubMed: 26073941]
22. Mohamed E, et al. The Unfolded Protein Response Mediator PERK Governs Myeloid Cell-Driven Immunosuppression in Tumors through Inhibition of STING Signaling. Immunity. 2020; 52 :668–682. e667 [PubMed: 32294407]
23. Batista A, et al. IRE1alpha regulates macrophage polarization, PD-L1 expression, and tumor survival. PLoS Biol. 2020; 18 e3000687 [PubMed: 32520957]
24. Heinzer S, Worz S, Kalla C, Rohr K, Weiss M. A model for the self-organization of exit sites in the endoplasmic reticulum. J Cell Sci. 2008; 121 :55–64. [PubMed: 18073241]
25. Zhang L, et al. Single-Cell Analyses Inform Mechanisms of Myeloid-Targeted Therapies in Colon Cancer. Cell. 2020; 181 :442–459. e429 [PubMed: 32302573]
26. Lambrechts D, et al. Phenotype molding of stromal cells in the lung tumor microenvironment. Nat Med. 2018; 24 :1277–1289. [PubMed: 29988129]
27. Maynard A, et al. Heterogeneity and targeted therapy-induced adaptations in lung cancer revealed by longitudinal single-cell RNA sequencing. bioRxiv. 2019; doi: 10.1101/2019.12.08.868828
28. Sanderson SM, et al. The Na⁺/K⁺ ATPase Regulates Glycolysis and Defines Immunometabolism in Tumors. bioRxiv. 2020; doi: 10.1101/2020.03.31.018739
29. Liu PS, et al. alpha-ketoglutarate orchestrates macrophage activation through metabolic and epigenetic reprogramming. Nat Immunol. 2017; 18 :985–994. [PubMed: 28714978]

30. Etzerodt A, et al. Specific targeting of CD163(+) TAMs mobilizes inflammatory monocytes and promotes T cell-mediated tumor regression. J Exp Med. 2019; 216 :2394–2411. [PubMed: 31375534]
31. Movahedi K, et al. Different tumor microenvironments contain functionally distinct subsets of macrophages derived from Ly6C(high) monocytes. Cancer Res. 2010; 70 :5728–5739. [PubMed: 20570887]
32. Yan D, Wang HW, Bowman RL, Joyce JA. STAT3 and STAT6 Signaling Pathways Synergize to Promote Cathepsin Secretion from Macrophages via IRE1alpha Activation. Cell Rep. 2016; 16 :2914–2927. [PubMed: 27626662]
33. Herbeuval JP, Lelievre E, Lambert C, Dy M, Genin C. Recruitment of STAT3 for production of IL-10 by colon carcinoma cells induced by macrophage-derived IL-6. J Immunol. 2004; 172 :4630–4636. [PubMed: 15034082]
34. Liu Y, et al. Role for the endoplasmic reticulum stress sensor IRE1alpha in liver regenerative responses. J Hepatol. 2015; 62 :590–598. [PubMed: 25457211]
35. Erbay E, et al. Reducing endoplasmic reticulum stress through a macrophage lipid chaperone alleviates atherosclerosis. Nat Med. 2009; 15 :1383–1391. [PubMed: 19966778]
36. Rong X, et al. LXRs regulate ER stress and inflammation through dynamic modulation of membrane phospholipid composition. Cell Metab. 2013; 18 :685–697. [PubMed: 24206663]
37. Huang SC, et al. Cell-intrinsic lysosomal lipolysis is essential for alternative activation of macrophages. Nat Immunol. 2014; 15 :846–855. [PubMed: 25086775]
38. Su P, et al. Enhanced Lipid Accumulation and Metabolism Are Required for the Differentiation and Activation of Tumor-Associated Macrophages. Cancer Res. 2020; 80 :1438–1450. [PubMed: 32015091]
39. Lee WB, et al. Mincle-mediated translational regulation is required for strong nitric oxide production and inflammation resolution. Nat Commun. 2016; 7 :11322. [PubMed: 27089465]
40. Li C, et al. The Mincle/Syk/NF-kappaB Signaling Circuit Is Essential for Maintaining the Protumoral Activities of Tumor-Associated Macrophages. Cancer Immunol Res. 2020; 8 :1004–1017. [PubMed: 32532809]
41. Clement M, et al. Necrotic Cell Sensor Clec4e Promotes a Proatherogenic Macrophage Phenotype Through Activation of the Unfolded Protein Response. Circulation. 2016; 134 :1039–1051. [PubMed: 27587433]
42. Tanaka M, et al. C-type lectin Mincle mediates cell death-triggered inflammation in acute kidney injury. J Exp Med. 2020; 217 doi: 10.1084/jem.20192230
43. Williams SJ. Sensing Lipids with Mincle: Structure and Function. Front Immunol. 2017; 8 :1662. [PubMed: 29230225]
44. Halbleib K, et al. Activation of the Unfolded Protein Response by Lipid Bilayer Stress. Mol Cell. 2017; 67 :673–684. e678 [PubMed: 28689662]
45. Kast HR, Nguyen CM, Anisfeld AM, Ericsson J, Edwards PA. CTP:phosphocholine cytidylyltransferase, a new sterol- and SREBP-responsive gene. J Lipid Res. 2001; 42 :1266–1272. [PubMed: 11483628]
46. Hashidate-Yoshida T, et al. Fatty acid remodeling by LPCAT3 enriches arachidonate in phospholipid membranes and regulates triglyceride transport. Elife. 2015; 4 doi: 10.7554/eLife.06328
47. Jalil A, et al. Revisiting the Role of LXRs in PUFA Metabolism and Phospholipid Homeostasis. Int J Mol Sci. 2019; 20 doi: 10.3390/ijms20153787
48. Tavazoie MF, et al. LXR/ApoE Activation Restricts Innate Immune Suppression in Cancer. Cell. 2018; 172 :825–840. e818 [PubMed: 29336888]
49. Vitale I, Manic G, Coussens LM, Kroemer G, Galluzzi L. Macrophages and Metabolism in the Tumor Microenvironment. Cell Metab. 2019; 30 :36–50. [PubMed: 31269428]
50. Poli V, Camporeale A. STAT3-Mediated Metabolic Reprograming in Cellular Transformation and Implications for Drug Resistance. Front Oncol. 2015; 5 :121. [PubMed: 26106584]
51. Tcyganov EN, et al. Distinct mechanisms govern populations of myeloid-derived suppressor cells in chronic viral infection and cancer. J Clin Invest. 2021; doi: 10.1172/JCI145971

52. Ackerman D, Simon MC. Hypoxia, lipids, and cancer: surviving the harsh tumor microenvironment. Trends Cell Biol. 2014; 24 :472–478. [PubMed: 24985940]
53. Thomas C, et al. LPCAT3 deficiency in hematopoietic cells alters cholesterol and phospholipid homeostasis and promotes atherosclerosis. Atherosclerosis. 2018; 275 :409–418. [PubMed: 29866392]
54. Martinez-Lopez M, et al. Microbiota Sensing by Mincle-Syk Axis in Dendritic Cells Regulates Interleukin-17 and -22 Production and Promotes Intestinal Barrier Integrity. Immunity. 2019; 50 :446–461. e449 [PubMed: 30709742]
55. Meeth K, Wang JX, Micevic G, Damsky W, Bosenberg MW. The YUMM lines: a series of congenic mouse melanoma cell lines with defined genetic alterations. Pigment Cell Melanoma Res. 2016; 29 :590–597. [PubMed: 27287723]
56. Yu YR, et al. Disturbed mitochondrial dynamics in CD8(+) TILs reinforce T cell exhaustion. Nat Immunol. 2020; 21 :1540–1551. [PubMed: 33020660]
57. Niwa H, Yamamura K, Miyazaki J. Efficient selection for high-expression transfectants with a novel eukaryotic vector. Gene. 1991; 108 :193–199. [PubMed: 1660837]
58. Driscoll WS, Vaisar T, Tang J, Wilson CL, Raines EW. Macrophage ADAM17 deficiency augments CD36-dependent apoptotic cell uptake and the linked anti-inflammatory phenotype. Circ Res. 2013; 113 :52–61. [PubMed: 23584255]
59. Ho PC, et al. Immune-based antitumor effects of BRAF inhibitors rely on signaling by CD40L and IFNgamma. Cancer Res. 2014; 74 :3205–3217. [PubMed: 24736544]
60. Ho PC, et al. Phosphoenolpyruvate Is a Metabolic Checkpoint of Anti-tumor T Cell Responses. Cell. 2015; 162 :1217–1228. [PubMed: 26321681]
61. Cox B, Emili A. Tissue subcellular fractionation and protein extraction for use in mass-spectrometry-based proteomics. Nat Protoc. 2006; 1 :1872–1878. [PubMed: 17487171]
62. Tsugawa H, Kanazawa M, Ogiwara A, Arita M. MRMPROBS suite for metabolomics using large-scale MRM assays. Bioinformatics (Oxford, England). 2014; 30 :2379–2380.
63. Checa A, et al. Hexosylceramides as intrathecal markers of worsening disability in multiple sclerosis. Mult Scler. 2015; 21 :1271–1279. [PubMed: 25480867]
64. Durinck S, et al. BioMart and Bioconductor: a powerful link between biological databases and microarray data analysis. Bioinformatics (Oxford, England). 2005; 21 :3439–3440.

Europe PMC Funders Author Manuscripts

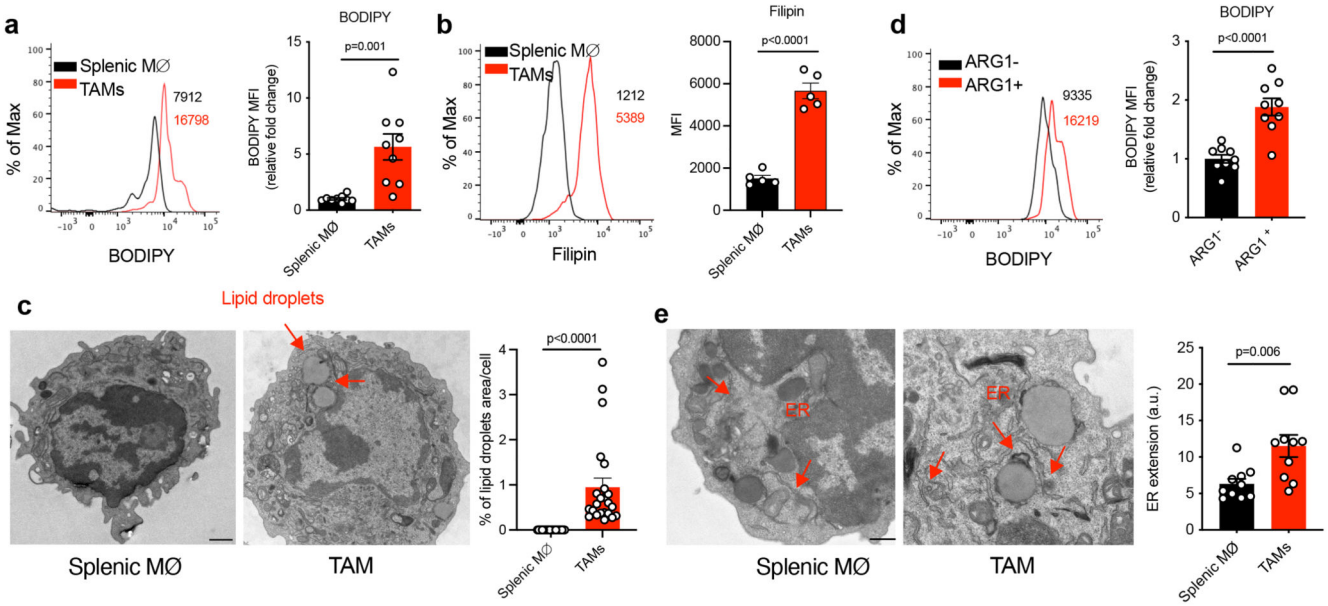

Figure 1. The TME promotes lipid accumulation in pro-tumorigenic TAMs.

a,**b**, Representative histogram (left) and quantitative plot of the geometric mean fluorescence intensity (MFI) (right) of BODIPY (**a**) and Filipin III (indicated as Filipin) (**b**) in splenic macrophages or tumor-associated macrophages (TAMs) of YUMM1.7 melanoma-bearing mice (n=9 per group in **a**; n=5 per group in **b**). **c**, Representative electron microscope images (left) and quantification (right) of lipid droplet formation in sorted TAMs and splenic macrophages (n=23 per group), Scale bar, 1μM. **d**, Representative histogram (left) and quantitative plots of the MFI (right) of BODIPY staining in TAMs gated based on ARG1 expression (n=9 per group). **e**, Representative electron microscope images (left) and quantitative plot (right) of ER extension in splenic macrophages and TAMs of YUMM1.7 melanoma-bearing mice (n=10 per group), scale bar, 200nm. Data are pooled from two independent experiments (**a-b**, **d)**. Data derived from one electron microscopy experiment (**c**, **e)**. Each symbol represents one individual. All data are mean ± s.e.m and were analysed by two-tailed, unpaired Student's t-test.

Europe PMC Funders Author Manuscripts

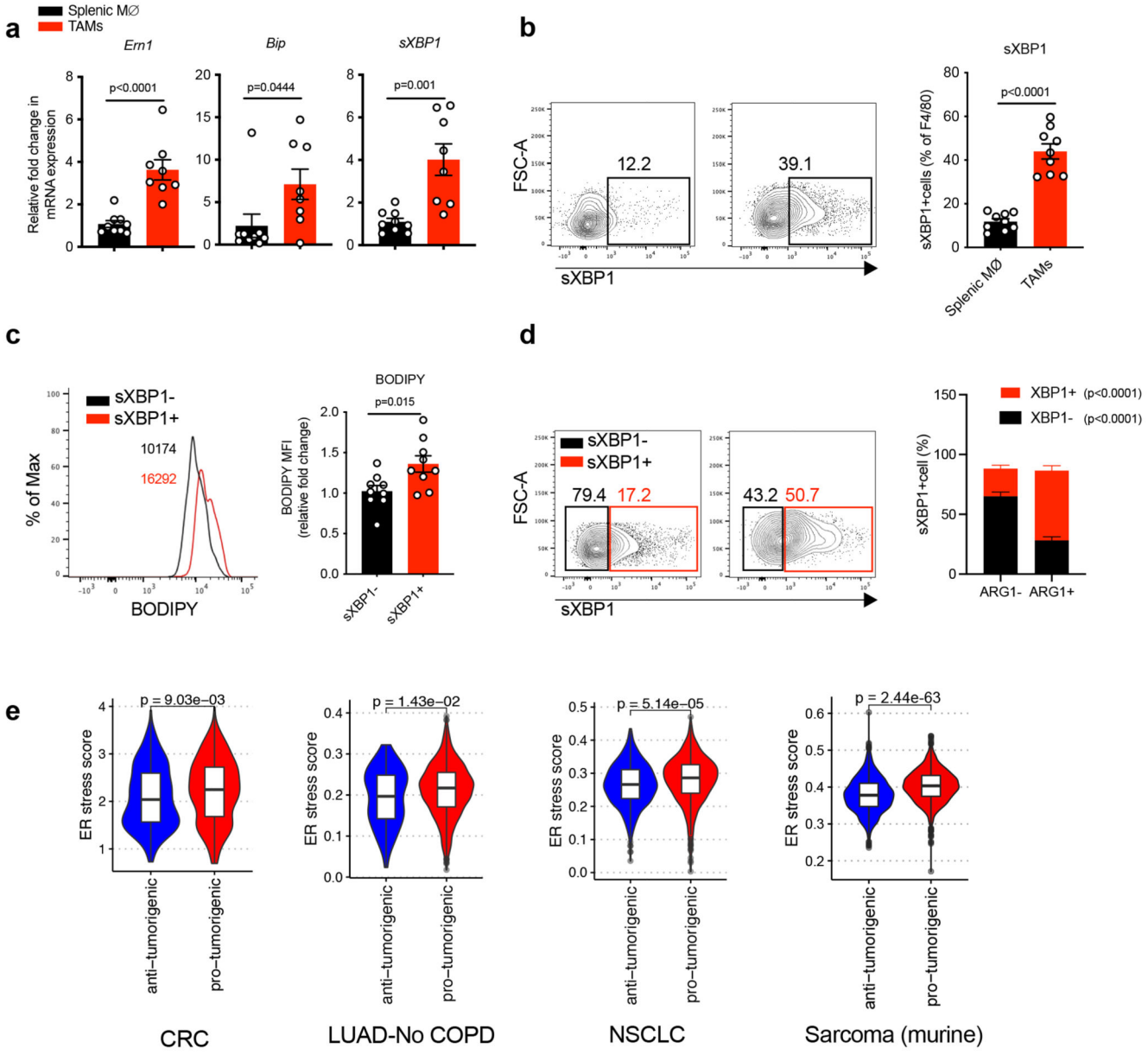

Figure 2. The TME activates IRE1/sXBP1 in pro-tumorigenic TAMs.

a, qPCR analysis of mRNA expression of indicated genes in splenic macrophages (n=9) and TAMs (n=8) isolated from YUMM1.7 melanoma-bearing mice. **b**, Representative histogram (left) and quantitative plot of the percentage (right) of sXBP1^{+} cells among splenic macrophages and TAM of YUMM1.7 melanoma-bearing mice (n=9 per group). **c,** Representative histogram (left) and quantitative plot of the MFI (right) of BODIPY staining in TAMs gated based on sXBP1 expression (n=9 per group). **d,** Representative histogram (left) and quantitative plot of the percentage (right) of sXBP1^{+} cells among ARG1^{+} and ARG1^{-} TAMs (n=9 per group). **e**, Violin plot and box plot show distributions of ER stress scores in anti-tumorigenic and pro-tumorigenic macrophages from different human and murine cancer types. Data are pooled from at least two independent experiments.

Europe PMC Funders Author Manuscripts

Each symbol represents one individual. All data are mean ± s.e.m and were analysed by two-tailed, unpaired Student's t-test (**a-d**), one-tailed unpaired Student's t-test (**e**). Box plot where whiskers represent the 5 and 95th percentile values, box limits represent the 25th and 75th percentiles, black line represents the median (**e**).

Europe PMC Funders Author Manuscripts

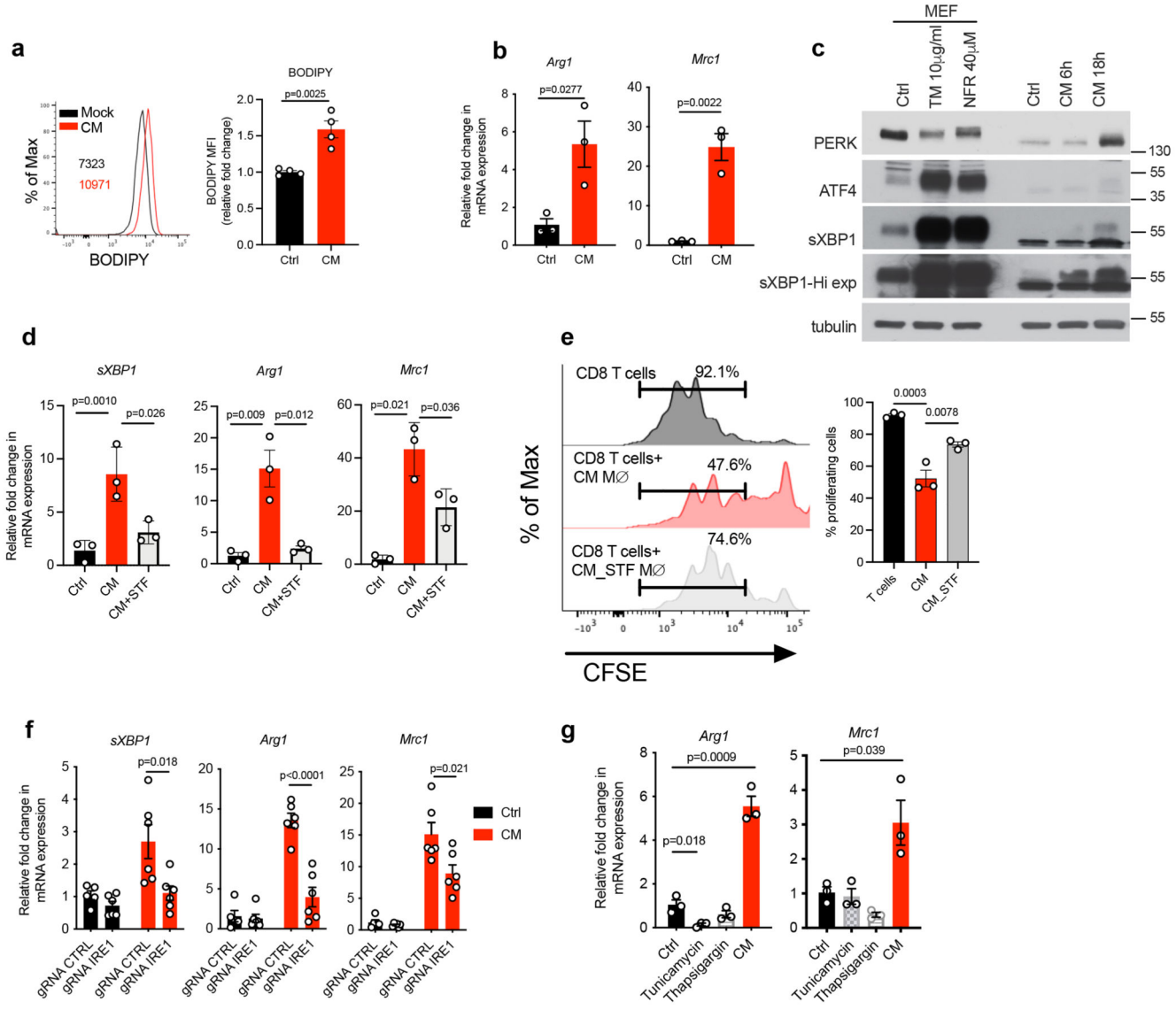

Figure 3. Tumor cells drive pro-tumorigenic polarization in BMDMs via IRE1.

a,b, BMDMs were cultured in regular culture medium (Ctrl) or in presence of YUMM1.7 melanoma cell-conditioned medium (CM) for 18h. Flow cytometry analysis was performed to analyse lipid content with n= 4 per group (**a**) or quantitative analysis of the expression of indicated genes with n= 3 per group (**b**). Data are representative results of three independent experiments. **c,** Immunoblots of indicated proteins in BMDM treated with indicated conditions and mouse embryonic fibroblasts (MEFs) treated with Tunicamycin (TM) or Nelfinavir (NFR) at the indicated doses as positive controls. Data are representative results of two independent experiments. **d,** qPCR analysis of mRNA expression of indicated genes in BMDMs stimulated with control medium (Ctrl), YUMM1.7 CM in the presence of 50μM STF081030 (CM+STF) or control vehicle (CM). Data are representative results of three independent experiments with n= 3 per group. **e,** Proliferation of carboxyfluorescein succinimidyl ester (CFSE)-labelled T cells activated with anti-CD3 and anti-CD28 alone

Europe PMC Funders Author Manuscripts

or in co-culture with BMDM previously exposed to CM or CM in presence of 50μM STF for 24h, in a ratio 2:1 (n=3 per group). Data are representative of three independent experiments. **f,** qPCR analysis of mRNA expression of indicated genes in control or IRE1-deficient BMDMs transduced with YUMM1.7 CM. Data are pooled from two independent experiments from four independent repeats (n=5 or 6 per group). **g,** qPCR analysis of mRNA expression of indicated genes in BMDM treated with tunicamycin, thapsigargin or YUMM1.7 CM for 16h. Data are representative results of three independent experiments with n= 3 per group. All data are mean ± s.e.m. and were analysed by two-tailed, unpaired Student's t-test (**a-b**, **d**, **f-g**) or one-way ANOVA with Tukey's multiple comparison test (**e**).

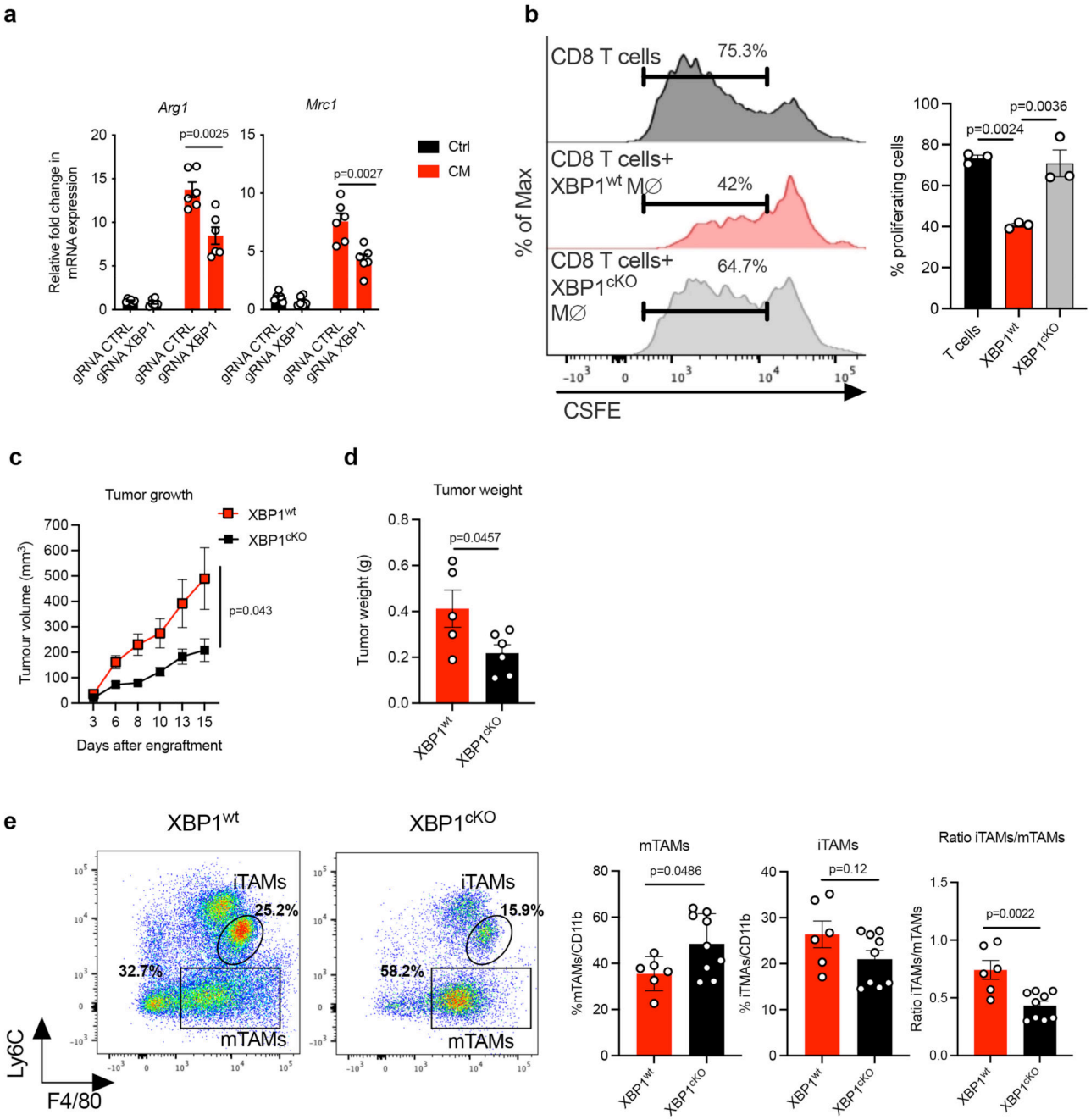

Figure 4. Deletion of XBP1 in TAMs suppresses tumor growth.

a, qRT-PCR analysis of indicated genes in Cas9-expressing BMDM transduced with retrovirus expressing gRNA targeting control or XBP1 sequence and exposed to Ctrl or CM (n=6 per group). Data are pooled from two independent experiments and repeated four times. **b,** Proliferation of CFSE-labelled T cells activated with anti-CD3 and anti-CD28 alone or in co-culture with BMDM isolated from wild type (XBP1^{wt}) or XBP1^{cKO} mice and previously exposed to CM in a ratio 2:1 (n=3 per group). Data are representative of three independent experiments. **c,d,** Tumor growth (**c**) and tumor weight (**d**) of YUMM1.7-

OVA melanoma from XBP1^{wt} (n=5) or XBP1^{cKO} (n=6) mice. Data are representative of three independent experiments. **e,** Representative plots (left) and percentages of iTAMs and mTAMs cells among CD11b+ myeloid cells in tumor-bearing XBP1^{wt} (n=6) and XBP1^{cKO} (n=9) mice. Data are pooled from two independent experiments. Each symbol represents one individual. All data are mean ± s.e.m. and were analysed by two-tailed, unpaired Student's t-test (**a**, **c-e**) or one-way ANOVA with Tukey's multiple comparison test (**b**).

Europe PMC Funders Author Manuscripts

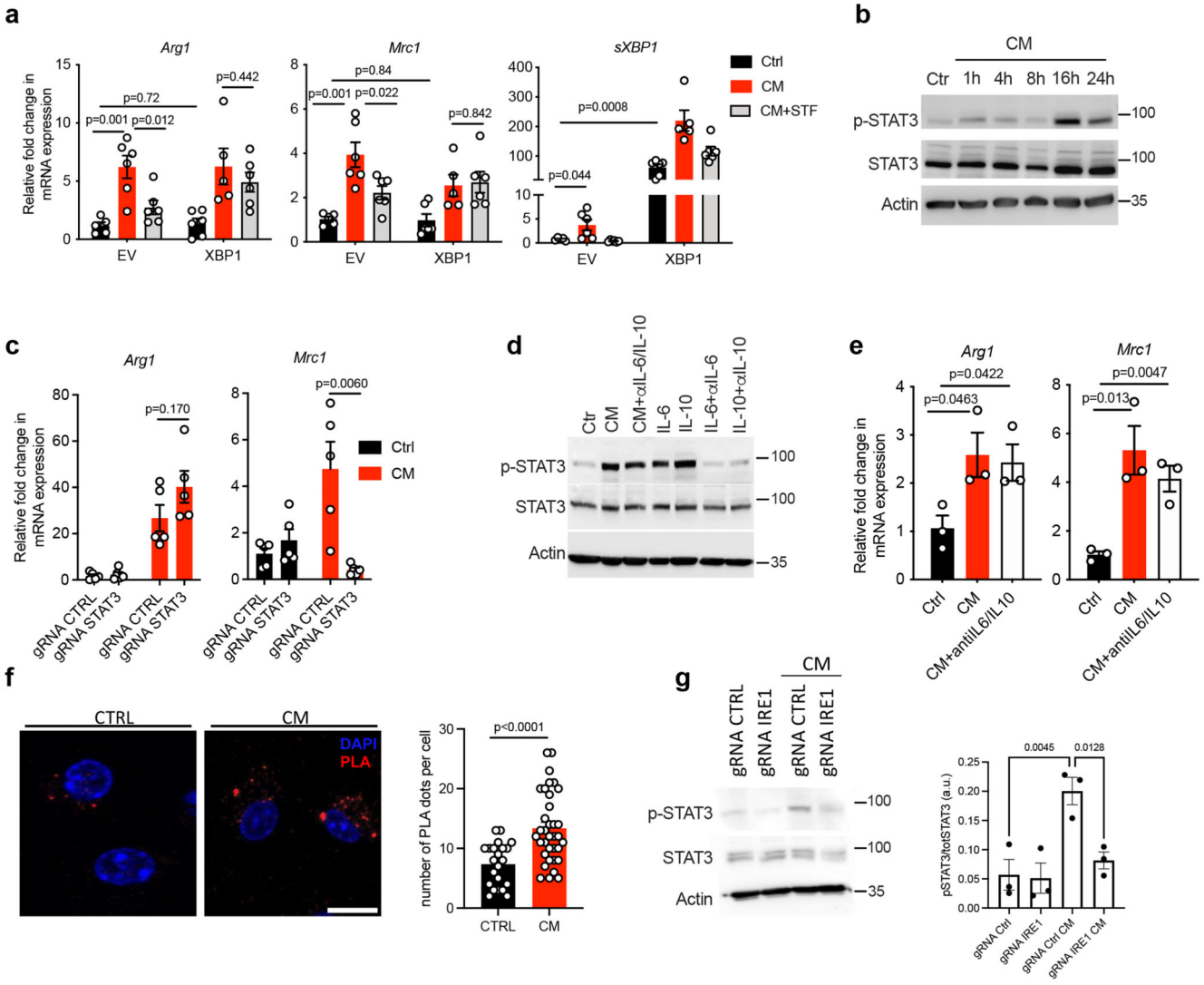

Figure 5. Activation of IRE1-STAT3 signal supports CM-induced polarization.

a, qPCR analysis of mRNA expression of indicated genes in BMDMs stimulated with YUMM1.7 CM in the presence of 50μM STF081030 (CM+STF) or vehicle (CM) BMDMs transduced with retrovirus expressing empty vector (EV) or sXBP1(sXBP1) as indicated in method; (*n*=6 per group for EV-CM, EV-CM-STF, XBP1-Ctrl and XBP1-CM-STF), EV-Ctrl (*n*=5), XBP1-CM (*n*=5). Data are pooled from two independent experiments and repeated four times. **b,** Immunoblots of BMDMs treated with CM for indicated duration. Data are representative results of three independent experiments. **c,** qPCR analysis of mRNA expression of indicated genes in BMDMs stimulated with control medium or YUMM1.7 CM (*n*=5 per group). BMDMs were transduced with retrovirus expressing control or STAT3-targeting gRNAs. Data are pooled from two independent experiments and repeated four times. **d,** Immunoblots of indicated proteins in BMDMs treated with indicated treatments. Ctrl: control medium; CM: YUMM1.7 conditioned medium; IL6: IL-6 treatment (10ng/ml); IL10: IL-10 treatment (10ng/ml). Anti-IL-6/IL-10 antibodies were added alone or in combination (0.25μg/ml anti-IL-6 and 0.25μg/ml anti-IL-10). Data

Europe PMC Funders Author Manuscripts

Europe PMC Funders Author Manuscripts

are representative results of three independent experiments. **e,** qPCR analysis of mRNA expression of indicated genes in BMDMs treated with CM in the absence or presence of 0.25μg/ml anti-IL-6 and anti-IL-10 antibodies (n= 3 per group). Data are representative results of three independent experiments. **f,** Representative images (left) and quantification (right) of proximity ligation assay (PLA) of BMDM exposed to Ctrl or CM for 18h, scale bar 10μM. Data are representative of two independent experiments: Ctrl (n=22), CM (n=35). **g,** Immunoblots (left) and quantification (right) (n=3 per group) of indicated proteins in control or IRE1-targeting gRNA expressing BMDMs stimulated with control medium (Ctrl) or YUMM1.7 CM (CM). Data are representative results of three independent experiments. All data are mean ± s.e.m. and were analysed by two-tailed, unpaired Student's t-test (**a**, **c, e**, **f**) or one-way ANOVA with Sidak's multiple comparison test (**g**).

Europe PMC Funders Author Manuscripts

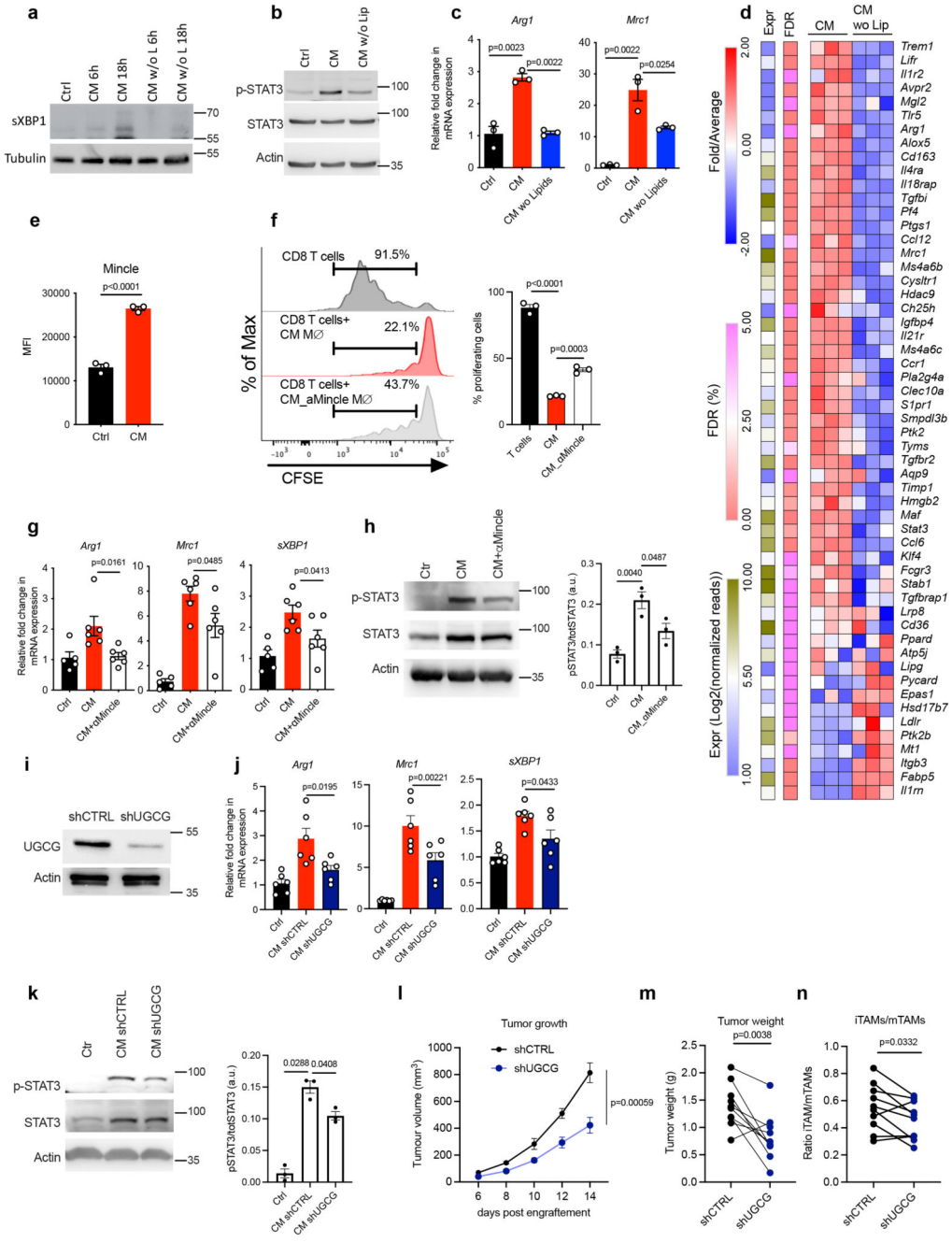

Figure 6. Mincle-dependent glucosylceramide sensing pathway tailors macrophage activation.

a-c, Immunoblots of indicated proteins (**a** and **b**) and qPCR analysis of indicated genes (**c**) in BMDMs treated with control medium (Ctrl), CM or CM without lipids for the indicated time points (**a**) or for 18h (**b** and **c**) (n=3 sample per group in (**c**)). Data are representative results of three independent experiments. **d,** Heatmap of mRNA expression of pro-tumorigenic genes, upon exposure of CM or CM without lipids, in BMDMs (n=3 per group). **e,** Quantitative plot of Mincle protein expression in BMDMs treated with control medium (Ctrl) or CM (n=3). Data are representative results of three independent

experiments. **f,** Proliferation of CFSE-labelled T cells activated with anti-CD3 and anti-CD28 alone or in co-culture with BMDM previously treated with CM or with CM in presence of 5μg/ml anti-Mincle antibody in a ratio 2:1 for 72h (*n*=3). Data are representative of three independent experiments. **g,h,** qPCR analysis of indicated genes (**g**) (*n*=5 or 6) and immunoblots of indicated proteins (left) with quantification (right) (*n*=3) (**h**) in BMDMs cultured with control medium (Ctrl) or CM in the absence or presence of 5μg/ml αMincle antibody. Data are pooled from two independent experiments and repeated four times in (**g**) and three times in (**h**). **i**, immunoblot of indicated proteins in YUMM1.7 cells shCTRL or shUGCG. **j,** qPCR analysis of indicated genes in BMDMs exposed to CM derived from YUMM1.7 shCTRL or YUMM1.7 shUGCG (n=6). Data are pooled from two independent experiments and repeated four times. **k**, immunoblots of indicated proteins (left) and quantification (right) of BMDMs cultured with CM from shCTRL or shUGCG YUMM1.7 (*n*=3). **l-n,** Tumor growth curve (**l**) and tumor weight (**m**) of YUMM1.7 shCTRL and YUMM1.7 shUGCG tumors in co-engrafted mice (*n*=10). Ratio of iTAMs/mTAMs from the indicated tumors of tumor-bearing mice (*n*=10) (**n**). Data are pooled from two independent experiments. Each symbol represents one individual. Data are mean ± s.e.m. and were analysed by two-tailed (**c, e, g, j**), unpaired Student's t-test or paired t-test (**m-n)** and one-way ANOVA with Tukey's multiple comparison test **(f, h,**) and RM one-way ANOVA with Sidak's multiple comparison test (k).

Europe PMC Funders Author Manuscripts

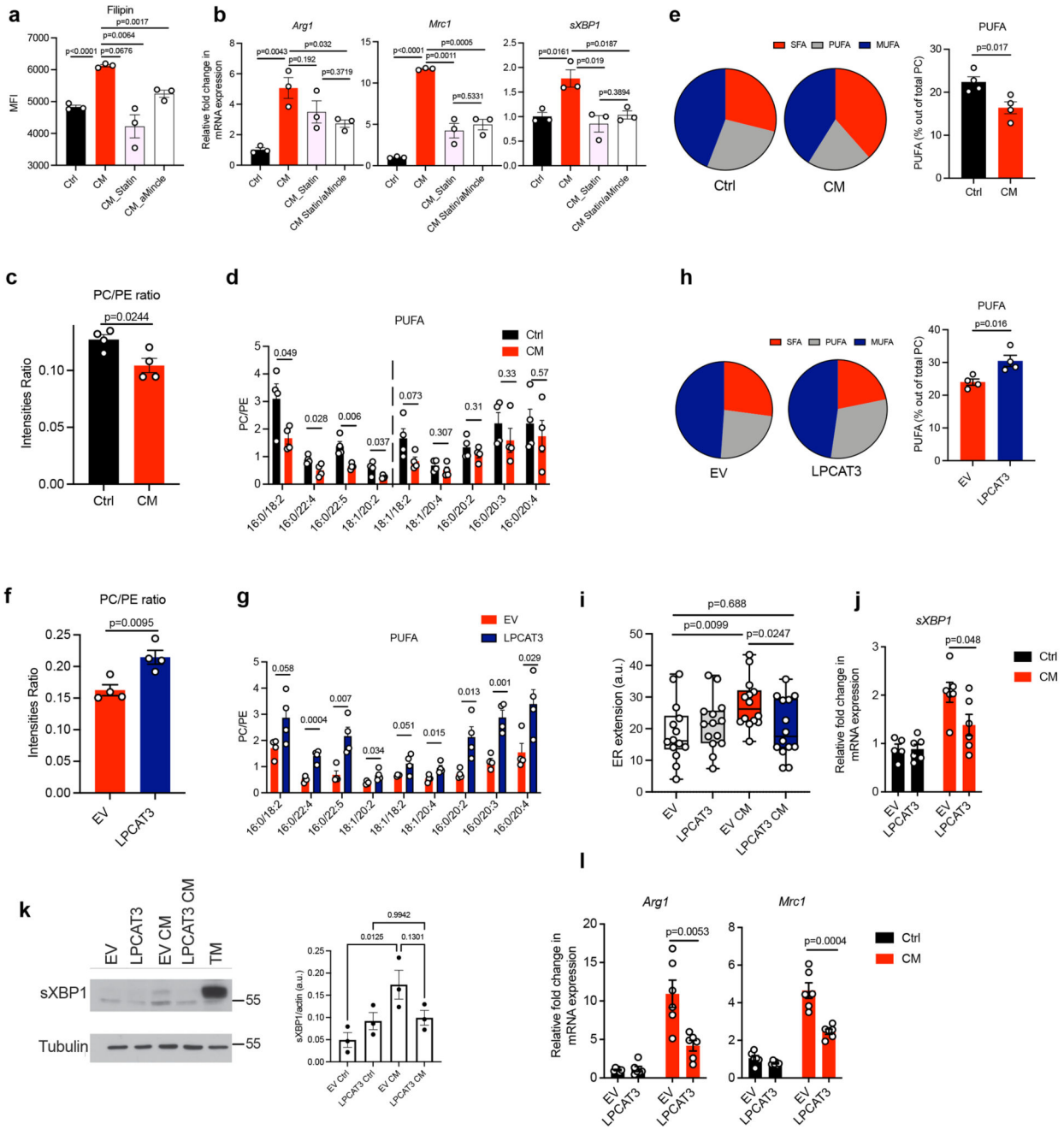

Figure 7. CM causes reshuffling of lipid composition and saturation of ER membrane.

a, MFI of Filipin III staining in BMDMs treated with CM or CM in presence of simvastatin (10μM) or αMincle antibody (5μg/ml) (n=3). **b**, qPCR analysis of indicated genes in BMDMs stimulated with control medium (Ctrl) or CM in presence of simvastatin (10μM) alone or with αMincle antibody (5μg/ml) (n=3). Data are representative results of at least two independent experiments. **c-e,** LC-MS/MS lipidomics performed on the endoplasmic reticulum membrane isolated from BMDMs exposed to control medium (Ctrl) or CM (n=4 per group). The ratio of the absolute value of whole phosphatidylcholine (PC) and

phosphatidylethanolamine (PE) species (**c**), the ratio PC/PE of single lipid species with polyunsaturated fatty acid chain (**d**), and the pie plot (left panel) and quantification result (right panel) showing the percentage of polyunsaturated fatty acid (PUFA) of PC species and their distribution compared to monounsaturated fatty acid (MUFA) and saturated fatty acid (SFA) (**e**). Data are pooled results of four independent replicates. **f-h,** LC-MS/MS lipidomics has been performed on the endoplasmic reticulum membrane isolated from empty vector (EV) or LPCAT3 overexpressing BMDMs treated with CM (n=4 per group). The ratio of the absolute value of whole phosphatidylcholine (PC) and phosphatidylethanolamine (PE) species (**f**), the ratio PC/PE of single lipid species with polyunsaturated fatty acid chain (**g**), and the pie plot (left panel) and quantification result (right panel) showing the percentage of polyunsaturated fatty acid (PUFA) of PC species and their distribution compared to monounsaturated fatty acid (MUFA) and saturated fatty acid (SFA) (**h**). Data are pooled results of four independent replicates. **i,** Quantitative plot of ER extension detected by electron microscopy in empty vector (EV) or LPCAT3 overexpressing BMDMs stimulated with control medium (Ctrl) or CM (n=14 per group). **j-l**, qPCR analyses of mRNA expression of indicated genes (**j** and **l**) (n=5 or 6) and immunoblot and quantification of indicated proteins (**k**) in EV or LPCAT3 overexpressing BMDMs stimulated with control medium (Ctrl) or CM (n=3). Data are representative results of three independent experiments. Data are mean ± s.e.m. and were analysed by two-tailed, unpaired Student's t-test (**a-j, i**) and one-way ANOVA with Sidak's multiple comparison test (**k**). Box plot where whiskers represent the min and max values, box limits represent the min and max values, black line represents the median (**i**).

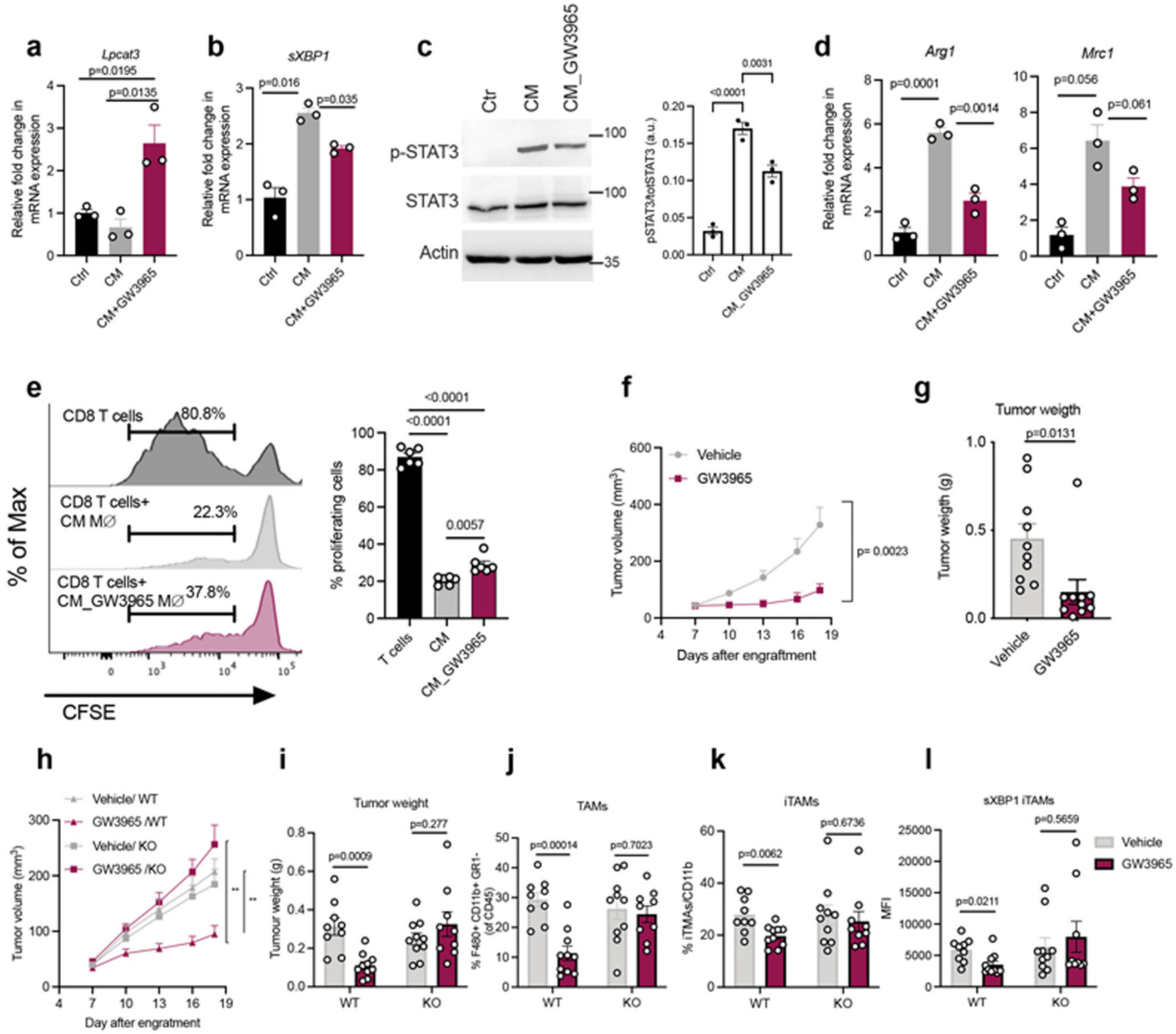

Figure 8. LXR agonist reduces tumor burden and hampers TAM survival in a LPCAT3-dependent manner.

a-d, qPCR of mRNA expression of indicated genes (**a, b** and **d**) and immunoblots (left) and quantification (right) of indicated proteins (**c**) in BMDMs stimulated with control medium (Ctrl) or CM in the absence or presence of GW3965 (3μM) (*n*=3). Data are representative results of three independent experiments. **e,** Proliferation of CFSE-labelled T cells activated with anti-CD3 and anti-CD28 alone of in co-cultured with BMDM previously treated with CM or with CM in presence of GW3965 in a ratio 2:1 for 72h (*n*=6). Data are pooled of three independent experiments. **f,g,** Tumor growth (**f**) and tumor weight (**g**) of YUMM1.7-OVA melanoma treated with either control vehicle or GW3965 (*n*=10 per group). Data are pooled from 2 independent experiments. **h-l,** Lethally irradiated C57BL/6 mice were transplanted with WT (LPCAT3 $^{fl/fl}$) or KO (LysM-Cre LPCAT3$^{fl/fl}$) BM cells. 7 weeks post bone marrow transplantation, mice were engrafted with YUMM1.7-OVA melanoma cells

and then treated with control vehicle or GW3965. Tumor growth (**h**) and tumor weight (**i**) of YUMM1.7-OVA melanoma were monitored (WT+Vehicle: n=9; WT+GW3965: n=10; KO+Vehicle: n=10; KO+GW3965: n=9). On day 18 post tumor engraftment, the percentage of total TAMs (**j**), iTAMs (**k**) and MFI of sXBP1 in iTAMs (**l**) in YUMM1.7-OVA melanomas were measured by flow cytometry. Data are pooled from two independent experiments. Each symbol represents one individual. All data are mean ± s.e.m and were analysed by two-tailed, unpaired Student's t-test (**a-b, d, f-l**) and one-way ANOVA with Tukey's multiple comparison test (**c, e**).

Europe PMC Funders Author Manuscripts